FCP Report No. 43

LOW CYCLE TORSIONAL FATIGUE OF 1045 STEEL IN SHEAR STRAIN CONTROL

By

Gail E. Leese

Department of Theoretical and Applied Mechanics

A Report of the

FRACTURE CONTROL PROGRAM

College of Engineering, University of Illinois
Urbana, Illinois 61801

September 1982

ABSTRACT

An experimental technique is established for performing strain controlled fatigue tests in torsion on thin-walled tubular specimens. The results of such tests on a 1045 hot rolled and normalized steel are reported. Fatigue crack initiation properties are determined in a manner analagous to the method used with axial fatigue data reduction.

Mode II (inplane shear) surface cracks are observed throughout a significant portion of the life of the 1045 specimens. Often, many cracks are observed that have no apparent effect on the final failure. This phenomenon is documented with surface replication techniques.

Finally, for the steel tested, it is established that the fatigue strength exponent, fatigue ductility exponent and cyclic strain hardening exponent are essentially the same in torsional and axial loading modes.

ACKNOWLEDGMENT

The experimental portion of this investigation was conducted in the Engineering Mechanics Department at the Deere & Company Technical Center, Moline, Illinois, with Dr. H. D. Berns as Manager. Much research was conducted in residence at the Department of Theoretical and Applied Mechanics, University of Illinois, Urbana, with Professor R. T. Shield as Department Head. Partial financial support was provided by the Fracture Control Program, College of Engineering, University of Illinois.

The author gratefully acknowledges the technical direction, input and patience of Professor JoDean Morrow. Also, the author sincerely appreciates the many stimulating coversations, invaluable ideas and aid offered by D. R. Galliart, S. D. Downing, and G. L. Curless throughout this investigation.

Ms. D. B. Cotter and Ms. L. K. Popp are thanked for typing the manuscript. Mr. M. A. Kelley and Mr. J. E. White are thanked for their aid with the figures. Mr. R. H. Meinke is recognized for skillfully machining the experimental samples and special devices.

TABLE OF CONTENTS

LIST OF SYMBOLS

σ_b	Applied bending stress
τ	Applied shear stress
B	Endurance limit in pure bending
T	Endurance limit in pure shear
σ_1, σ_2, σ_3	Alternating principal stress amplitudes
S_x, S_y, S_z	Orthogonal mean stresses in Sines' approach
A, α	Materials properties for a given lifetime in Sines' approach
τ_{oct}	Octahedral shear stress
$\Delta\varepsilon$	Total strain range
$\Delta\varepsilon_e$	Elastic strain range
$\Delta\varepsilon_p$	Plastic strain range
σ_f'	Fatigue strength coefficient
b	Fatigue strength exponent
ε_f'	Fatigue ductility coefficient
c	Fatigue ductility exponent
E	Modulus of elasticity
N	Number of cycles
2N	Number of reversals
$2N_f$	Number of reversals to failure
$2N_t$	Transition fatigue life
ε_{eq}	Equivalent plastic strain amplitude
ε_1, ε_2, ε_3	Alternating principal strain amplitudes
λ	σ_2/σ_1
ν	Poisson's ratio
$\Delta\varepsilon_1$	Maximum principal strain range

m	Material parameter in Mowbray's approach
$f(\lambda,\upsilon)$	Function relating principal elastic strain range to the effective range in Mowbray's approach
$g(\lambda,m)$	Function relating principal plastic strain range to the effective range in Mowbray's approach
σ_a	True stress amplitude
K'	Cyclic strength coefficient
n'	Cyclic strain hardening exponent
$\Delta\gamma$	Total shear strain range
$\Delta\gamma_e$	Elastic shear strain range
$\Delta\gamma_p$	Plastic shear strain range
G	Modulus of elasticity in shear
τ_f'	Fatigue shear strength coefficient
b_o	Fatigue shear strength exponent
γ_f'	Fatigue shear ductility coefficient
c	Fatigue shear ductility exponent
τ_a	True shear stress amplitude
K_o'	Cyclic shear stress coefficient
n_o'	Cyclic shear strain hardening exponent
T	Torque
R_i	Inner radius of test specimen
R_o	Outer radius of test specimen
R_m	Mean radius of test specimen
t	Wall thickness of test specimen
θ	Angle of twist per unit length

LIST OF TABLES

LIST OF FIGURES

I. INTRODUCTION

A. Overview

Historically, there have been two approaches to dealing with the phenomenon of metal fatigue in terms of analytical representation and design criteria. The first, the "endurance" or "infinite life" approach attempts to define the stress limits below which failure will never (for all practical purposes) occur. Baseline values for an endurance limit can be obtained in the laboratory and applied as a design criterion to components that are subjected to low amplitude loads.

The second, and most recently developed, is the "finite life" approach. Qualitatively, it may be thought of as a refinement of the endurance limit approach with the end goal of providing finite fatigue life prediction methods. Although the testing and analysis is different than that to determine endurance limits, baseline fatigue properties are obtained in the laboratory. These properties may then be used in conjunction with representative service or loading histories to predict the fatigue crack initiation lives of components in service. It should be added that the finite life approach has been extended to permit estimates of the fatigue crack propagation lives as well.

In the finite life approach, the baseline fatigue properties are obtained from laboratory specimens tested in uniaxial strain controlled tension-compression cyclic tests. The accuracy of the analytical methods using these properties has been verified only for uniaxial conditions. Since multiaxial loading environments are present in many actual machine parts, it is necessary either to reduce the stress state into a manageable form for comparison with uniaxial properties, or to obtain baseline fatigue properties in stress states other than uniaxial. The research included in this thesis is meant to provide input in addressing this point.

B. Background: Fatigue Failure Criteria

Most early work in fatigue is based on the endurance limit approach where, in the case of uniaxial fatigue, an equivalent stress value is defined below which failure will not occur. In general, the extension of this approach to multiaxial loading (monotonic or cyclic) requires defining an "effective" or "equivalent stress", i.e., reducing the multiaxial stress state to a scalar such that it can be compared with uniaxial data. Any one equivalent stress criteria can be illustrated as a surface or "envelope" in stress space within which failure will not occur. Often the equivalent stress is defined as the yield strength in a monotonic tension test; hence these criteria plotted in stress space represents yield surfaces. Figure 1 shows some common equivalent stress criteria plotted in two dimensional principal stress space.

Gough[1]* pioneered much work in the area of biaxial endurance limits with test programs ranging from pure bending to pure torsion. He fit his data from two ductile steels to an ellipse with the minor axis representing the endurance limit in pure bending and the major axis representing the endurance limit in pure torsion. This ellipse is represented by

$$\left(\frac{\sigma_b}{B}\right)^2 + \left(\frac{\tau}{T}\right)^2 = 1 \qquad (1)$$

where: B = endurance limit in pure bending

T = endurance limit in pure shear

σ_b = applied bending stress

τ = applied shear stress

Note that by varying the ratio of the shear to bending endurance limits the ellipse is reduced to different equivalent stress criteria, according to the following:

$T/B = .58$	von Mises distortion energy criterion
$T/B = .5$	Tresca maximum shear stress criterion

There are two major technical objections to the infinite life approach:

1. Some metals (e.g., aluminum) do not exhibit an endurance limit in constant amplitude laboratory tests.
2. Often, metals that do exhibit an endurance limit in constant amplitude tests do not in actual service applications. Just a few cycles of high strain may eradicate an endurance limit.

---

*Numbers in brackets refer to the list of references following the text.

Many other investigators, including Guest [2], Findley [3] and McDiarmid [4] have also proposed modifications of various equivalent stress criteria to account for multiaxial loading. Often these endurance limit approaches are used to predict finite lives by defining the mathematical constants at specific life levels. For example, by defining B and T in Eq. (1) as the bending and torsional strengths, respectively, at 10^5 reversals to failure one could derive a "Gough ellipse" for 10^5 reversals to failure rather than for infinite life.

Sines [5, 6] has done extensive work along these lines. He correlates fatigue life with the octahedral shear stress, corrected for any superimposed mean stress. Mathematically, this criterion can be expressed as:

$$1/3[(\sigma_1 - \sigma_2)^2 + (\sigma_2 - \sigma_3)^2 + (\sigma_3 - \sigma_1)^2]^{\frac{1}{2}} \leq A - \alpha\,(S_x + S_y + S_z) \qquad (2)$$

where: σ_1, σ_2, σ_3 = the alternating principal stresses

S_x, S_y, S_z = the orthogonal mean (or static) stresses

A, α = materials properties for a given life level

Note that the expression on the left-hand side of Eq. (2) is equivalent to the octahedral shear stress, τ_{oct}. Graphically, Sines' criterion is represented in plane stress space by a series of concentric ellipses. The interior of any one ellipse defines the region of permissible alternating stress at a given life level with given mean stresses. Qualitatively, Sines suggests that the octahedral shear stress criterion "averages" the effect of shear stresses on many different slip planes and that deviations from the criterion indicate the incompleteness of the averaging.

In fatigue analysis the above methods are useful primarily in the high cycle (low stress amplitude) regime for determining whether or not a fatigue problem exists. However, to make finite life predictions the low cycle fatigue response must be characterized in addition to more precisely quantifying the high cycle response.

The strain based approach as developed by Morrow and others[7, 8] has been found to be the most useful method for determining crack initiation life of wrought metals in uniaxial fatigue. Baseline materials properties are obtained from constant amplitude fully reversed strain controlled tests. Total strain range, $\Delta\varepsilon$, is the controlled parameter with stress amplitude, σ_a, elastic and plastic strain amplitudes, $\Delta\varepsilon_e/2$ and $\Delta\varepsilon_p/2$, respectively, measured from the cyclically stable stress-strain loop, Fig. 2. Reversals to failure, $2N_f$, as defined by a predetermined drop off in load, are also recorded. The elastic strain-life and plastic strain-life relationships have been found to fit a power law such that the functions are linear when plotted on a log-log scale. The total strain amplitude is related to life by summing the elastic and plastic components such that

$$\frac{\Delta\varepsilon}{2} = \frac{\Delta\varepsilon_e}{2} + \frac{\Delta\varepsilon_p}{2} \tag{3}$$

$$\frac{\Delta\varepsilon}{2} = \frac{\sigma_f'}{E}(2N_f)^b + \varepsilon_f'(2N_f)^c \tag{4}$$

where: σ_f' = fatigue strength coefficient

b = fatigue strength exponent

ε_f' = fatigue ductility coefficient

c = fatigue ductility exponent

$2N_f$ = reversals to failure

These relationships are shown graphically in Fig. 3.

Details of this type of strain-life analysis and its use in making life predictions of actual components which experience variable amplitude loading are presented in Reference [9]. Here it is appropriate to question how this uniaxial strain-life relationship can be applied to other modes of loading.

A frequent approach has been to modify Eq. (4) to account for multiaxial strains by defining an "effective strain range" to relate to life. Although the general form of the power law relationship still seems acceptable, there are conflicting opinions about which "effective" stress or strain parameter is appropriate.

Pascoe and deVilliers [10] investigated uniaxial, torsional and equibiaxial stress states using a mild steel. They measured life as a function of the equivalent plastic strain which, in turn, was related to principal strains.

$$\varepsilon_{eq} = \sqrt{\frac{2}{3}} \left[(\varepsilon_1 - \varepsilon_2)^2 + (\varepsilon_2 - \varepsilon_3)^2 + (\varepsilon_3 - \varepsilon_1)^2 \right]^{\frac{1}{2}} \quad (5)$$

In addition, they modified the fatigue ductility exponent to reflect the "state of strains."

Taira [11, 12, 13] found that the results of combined axial-torsion tests on a .16 percent C steel showed a good fit between von Mises' equivalent strain and life at elevated temperature. However, the Tresca equivalent strain showed a better correlation with life at room temperature.

Havard and Topper [14] used a maximum shear stress (Tresca) criterion, but added a hydrostatic stress modification. In a later paper [15] they changed to an octahedral shear strain parameter modified for the hydrostatic stress. In both cases they maintained a power law relationship between stress and life.

Mowbray [16] has suggested different modifications for the elastic and plastic strain-life relationships for the biaxial loading case. Qualitatively, the end result is a modification of the intercepts of the elastic and plastic strain-life lines (see Eq. (4) and Fig. 4) to account for the effects of biaxiality on fatigue strength and ductility, while maintaining the same slopes as in uniaxial fatigue. His biaxial criterion is represented as:

$$\frac{\Delta\varepsilon_1}{2} = f(\lambda,\nu)\,\frac{\sigma_f'}{E}\,(2N_f)^b + \frac{3}{3-m}\,g(\lambda,m)\,\varepsilon_f'(2N_f)^c \qquad (6)$$

where: $\frac{\Delta\varepsilon_1}{2}$ = maximum principal strain range

$\lambda = \frac{\sigma_2}{\sigma_1}$

ν = Poisson's ratio

m = material parameter weighting the effect of a hydrostatic stress component on plastic deformation

The function, $f(\lambda,\nu)$, relates the maximum principal elastic strain range to the effective range via the distortion energy theory. Equivalent plastic strain based on distortion energy and the von Mises plastic flow rule is related to the maximum principal plastic strain range by the function, $g(\lambda,m)$. The factor, $\frac{3}{3-m}$, was introduced as a modification to the uniaxial fatigue ductility coefficient, ε_f', to obtain a biaxial fatigue ductility coefficient. Note that a new material parameter, m, has been introduced in the expression for plastic strain. Mowbray suggests m is mathematically bounded in the interval $0 \leq m < 1.5$, with a realistic value of .7 for several engineering metals. It is also worth noting that Eq. (6) reduces to Eq. (4) in the case of uniaxial fatigue.

There is very little strain controlled fatigue data in a non-uniaxial mode available. Halford and Morrow [17] performed completely reversed plastic strain controlled torsion tests on two aluminum alloys, 60-40 brass and SAE 4340 steel. The only uniaxial data available for comparison are for an SAE 4142 quenched and tempered steel[18], with yield and ultimate strengths similar to the SAE 4340. Values of the fatigue strength exponent, b, correlate fairly closely with $b = -.088$ for 4340 in torsion and $b = -.081$ for 4142 in uniaxial fatigue. Values for c and n' do not compare as favorably, possibly because the torsional fatigue data were obtained from plastic strain rather than total strain controlled tests. Also, there are relatively few data points available from the torsional fatigue tests.

Benham[19, 20] performed axial and torsional strain controlled tests on pure copper in the annealed and cold-worked conditions. His data from each stress state show the fatigue ductility exponent, c, to be of slightly larger magnitude (i.e., a steeper negative slope in the plastic strain-life relationship) in the axial mode of fatigue. The values of c in the axial and shear modes, respectively, were -.58 and -.51 for the cold worked condition and -.54 and -.46 for the annealed copper.

C. Present Work

The experimental work presented here is constant amplitude shear strain controlled torsional low cycle fatigue data. It is analogous to uniaxial constant amplitude fatigue data, but obtained in a different loading mode. Although torsional fatigue is one-dimensional in loading, it is two-dimensional in stress state, hence it may be useful in judging whether or not uniaxial finite life fatigue properties can be extrapolated to determine response in a non-uniaxial environment. The primary question addressed here is whether the exponents in the power law fatigue relationships are constant from one stress state to the next.

As described in Eq. (4), the total strain-life relationship is a summation of the elastic strain-life

$$\frac{\Delta\varepsilon_e}{2} = \frac{\sigma_f'}{E} (2N_f)^b \qquad (7a)$$

and the plastic strain-life

$$\frac{\Delta\varepsilon_p}{2} = \varepsilon_f' (2N_f)^c \tag{7b}$$

relationships. Eliminating life from Eqs. 7(a) and (b), one obtains the cyclic stress versus plastic strain relationship

$$\sigma_a = K'(\varepsilon_p)^{n'} \tag{7c}$$

where: σ_a = true stress amplitude

K' = cyclic strength coefficient

and n' = cyclic strain hardening exponent

Hence, there are six baseline materials properties determined for low cycle fatigue analysis: σ_f', c_f', K', b, c and n', of which only four are independent. Mathematical and physical considerations dictate that

$$n' = \frac{b}{c} \tag{8a}$$

and

$$K' = \frac{\sigma_f'}{(\varepsilon_f')^{n'}} \tag{8b}$$

These constraints are often ignored in reducing fatigue data, but are a natural consequence of accurate results.

Equations 7(a) - (c) and 8(a) - (b) are expressed in uniaxial terms. Analogous relationships for the case of torsional fatigue can be expressed as follows:

$$\frac{\Delta\gamma_e}{2} = \frac{\tau_f'}{G} (2N_f)^b o \tag{9a}$$

$$\frac{\Delta\gamma_p}{2} = \gamma_f' (2N_f)^{c_o} \tag{9b}$$

$$\tau_a = K_o' (\gamma_p')^{n_o'} \tag{9c}$$

where: $\Delta\gamma_e$ = elastic shear strain range

$\Delta\gamma_p$ = plastic shear strain range

τ_a = true shear stress amplitude

τ_f' = fatigue shear strength coefficient

γ_f' = fatigue shear ductility coefficient

K_o' = cyclic shear strength coefficient

b_o = fatigue shear strength exponent

c_o = fatigue shear ductility exponent

n_o' = cyclic shear strain hardening exponent

Shear strain controlled fatigue test data are ideal for determining n', b and c in a non-uniaxial loading mode, since the choice of a strain parameter for use in the power law relationships in Eqs. 7(a) and 7(b) should have no effect on b and c, and therefore no effect on n'. For example, the differences between using a maximum principal strain-life, maximum shear strain-life and octahedral shear strain-life are merely scalar quantitites. They would affect the coefficients, but not the slopes of the power law relationships in Eqs. (7a) and (7b).

Assuming that in pure torsion, the total shear strain is the summation of the elastic and plastic shear strain, one arrives at the following relationships between total shear strain and life:

$$\frac{\Delta\gamma}{2} = \frac{\tau_f'}{G} (2N_f)^{b_o} + \gamma_f' (2N_f)^{c_o} \tag{10a}$$

and cyclic shear stress and shear strain

$$\frac{\Delta\gamma}{2} = \frac{\tau_a}{G} + \left(\frac{\tau_a}{K_o'}\right)^{1/n_o'} \tag{10b}$$

The purpose of this investigation is to determine whether or not $b = b_o$, $c = c_o$ and/or $n' = n_o$ for a 1045 hot rolled (HR) and normalized steel.

II. EXPERIMENTAL PROGRAM

A. Test and Specimen Design

There were two basic requirements considered in establishing the torsional fatigue test method:

1. Control of the total shear strain range within the gage length of deformation.
2. Capability of measuring total shear strain, shear stress amplitude, shear modulus and cycles to failure.

It was the second consideration that dictated specimen geometry. The use of a solid round specimen would present difficulties in directly calculating the shear stress at the surface after plastic yielding, when the stress distribution across the plane in torsion is nonlinear. Nadai[21] has presented a method of back calculating this stress for a solid round. A direct stress calculation from acquired load data can be made for a thin-walled tubular specimen assuming that the stress is constant across the thickness, and that the thickness of the wall is constant. Hence, a specimen with a thin-walled gage length was used. The ratio of wall thickness to the outer and inner diameter was .1 and .125, respectively. Note that the 4 mm wall thickness is of a dimension comparable to the axial specimens, which were 6 mm in diameter. Figure 4 shows the geometry and dimensions of the test specimen.

According to the thin-walled theory:

$$\tau = \frac{T}{2\Pi R_m^2 t} \tag{11}$$

where: T = torque

R_m = mean radius

t = wall thickness

This relationship is an approximation useful after plastic yielding has occurred. Considerable error would be introduced in applying Eq. (11) to elastic response, the amount of error depending on the difference between the outer and the mean radius. Hence, for modulus calculations during elastic reponse, the stress is calculated by:

$$\tau = \frac{T R_o}{(\Pi/2)(R_o^4 - R_i^4)}$$

where: R_o = outer radius

R_i = inner radius

The thin-walled approximation is used at all times after yielding has occurred.

Each specimen had a honed surface on the interior and a ground outer surface. Thus, the surfaces were not as finely polished as would be a smooth, round axial fatigue specimen, however, the grinding marks were perpendicular to the crack direction.

The test system used throughout this investigation is not commercially available, although most of the individual components are. The basic system was that designed by Galliart and Downing[22] for use in the biaxial fatigue program sponsored by the Society of Automotive

Engineers (SAE) Fatigue Design and Evaluation Committee. It included two independent linear actuators with two 10 kip load cells. The specimen was clamped into the test frame with a wedge-type fixture, and into the load arm with a collet. Most of the hardware was adapted from MTS materials test systems, including a computer interface to a PDP 11/04 allowing computer control of the two rams. Figures 5(a) and 5(b) show the testing apparatus.

In the SAE biaxial program, this test setup is used for load controlled combined bending/torsion tests. Hence, some hardware and software modifications were necessary to perform strain controlled tests in torsion.

To reduce the possibility of undesired bending, the load cell on actuator number two was slaved to the inverted signal from actuator number one directly through the internal hardware. Hence, at any point in time, each ram theoretically imparted loads of equal amplitude but opposite sign on the specimen to achieve pure torsional loading. In actuality, there was a slight time lag between the measuring of the load signal of ram number one and execution of the inverted signal by ram number two. Any continued resultant difference in load amplitudes between the rams would produce a cyclic bending stress. Typically, the bending stress was less than 2% of the shear stress range and considered negligible.

A method of measuring the shear strain over the gage length which could also be used as the feedback signal in the closed-loop control was needed. The "shear strain extensometer" devised[23] consisted of a Schaevitz R30D RVDT (rotary variable differential transducer) set into two sleeves, one holding the body of the RVDT and the other attached to the shaft, Figs. 6(a) and (b). Each sleeve consisted of two pieces separated by an O-ring. By tightening the two pieces together, each O-ring could be expanded against the I.D. of the specimen, thus internally mounting the RVDT between the two O-rings, within the gage length of the specimen. Figure 7 shows the position of the transducer during the test.

The RVDT produced a voltage output as a function of the angular position of the shaft. In this test procedure the RVDT output indicated the relative angular displacement between the O-rings. Since the angle of twist is directly related to the shear strain by the relationship:

$$\gamma = R_m \theta \tag{13}$$

control of the angle of twist per unit length, θ, over a given gage length is one means of controlling γ over that same gage length.

Unfortunately, the raw signal from the RVDT was not compatible with the strain conditioning module available on the MTS materials test stand which normally receives the output of a linear extensometer. A new conditioning module compatible with the RVDT and the MTS electronics was designed at the Deere & Company Technical Center[24] thus allowing not only measurement, but control of angular displacement through a closed

loop system. Finally, the console accepting the RVDT signal was operated in strain control, with the ram movements controlled within the computer software. The second console remained in load control such that the load cell on its associated ram remained slaved via the hardware to the other ram.

B. Material

The material chosen for this study was 1045 HR and normalized steel. The diameter of the bar stock was 63.5 mm. Inland Steel donated 8 tons of this steel from the same heat to the SAE Biaxial Program. LaSalle Steel performed the normalizing treatment. The material tested in this investigation was acquired from this SAE stock. Availability aside, this material was chosen because the results will be complementary to the SAE biaxial research currently underway.

Chemical composition of the steel is shown in Table I. Brinell hardness measurements from all specimens fell within the range of 192 to 201. The microstructure consisted of fine grained pearlite and ferrite, but also contained thin inclusions along the rolling direction up to .1 mm in length. Figure 8 shows the microstructure at 100X.

Tables II and III list the axial monotonic and fatigue properties from 6 mm diameter specimens, respectively. Axial strain-life curves are shown graphically in Fig. 9. The associated cyclic stress-strain curve superimposed on the monotonic, shown in Fig. 10, shows cyclic softening at low strain amplitudes and cyclic hardening at high strain amplitudes.

C. Torsional Fatigue Test

Each specimen was strain gaged with a three-legged rosette, placed approximately in the middle of the gage length. Prior to the fatigue tests each specimen underwent several single cycle tests at $\gamma_a \simeq .001$ to compare the RVDT and the rosette readings. Any initial disparity was due to the gage length input parameter used with the relative angle of twist to calculate the shear strain measured by the RVDT. In a sense, this method analytically "calibrated" the RVDT with the rosette.

The first and second fully reversed cycles to the desired shear strain amplitude of the test were also performed as single cycle tests. The RAMP test function of MTS Basic was used to control the linear strain response. In most cases, 100 samples/cycle were used to generate the RAMP signal. For the cycle of initial yield, 100 samples/cycle were also used for the data acquisition performed on the RVDT, load cells and rosette legs. After each single cycle the rams returned to a position of zero shear strain.

Generally, the fatigue test was initiated with the third cycle, again using 100 samples/cycle for generating the ramp. Data acquisition from the RVDT and the load cells was performed at the rate of 25 samples/cycle. These intervals were found satisfactory for all but the largest shear strain amplitude where they were increased to 200 and 50 samples/cycle for the ramp signal generation and data acquisition, respectively.

There were predetermined intervals during the fatigue tests at which data acquisition was performed and written to disk so that the stress-strain response could be regenerated at a later time. These intervals were at 1, 17, 33, 65, 129, 256 . . .etc., cycles, although immediate mode data acquisition could be performed on demand at any intermediate level.

Intermittently, during most fatigue tests, cellulose film replicas were made that were later examined under an ordinary light microscope for studying surface cracking. A microscope mounted on the frame of the test stand was also used to observe surface cracking. In all tests the life to failure was recorded.

Three specimens were tested at each of the following shear strain amplitudes: $\gamma_a = \pm.0250$, $\pm.0150$, $\pm.0080$, $\pm.0050$, and $\pm.0040$. One specimen was tested at $\gamma_a = \pm.0060$ before the strain amplitudes for testing were firmly established and the remaining specimen was tested at $\gamma_a = \pm.003$ to represent long life behavior.

One attempt to do a monotonic torsion test was made. The available test equipment was not adequate for twisting such a ductile material to failure in one cycle, hence only rather crude measurements were possible. The majority of the test was executed manually since the shear strain extensometer used in the fatigue tests did not have the range required for the monotonic test. There were several rectangular elements scribed on the sample prior to testing. At periodic load levels, replicas were made of the deformed rectangular elements. Dimensions of the deformed elements were then measured through a microscope and used to determine shear strain.

III. RESULTS

A. Fatigue Test Results

There were two distinctly different modes of failure observed in all tests; a shearing mode where longitudinal cracks formed followed by a mode where the faces of the longitudinal cracks opened and closed. Either mode in itself could be described in terms of initiation and propagation, with the propagation of longitudinal cracks in shear preceeding the initiation of opening and closing across the faces of the same cracks. Hence, defining the fatigue life to crack initiation cannot be done without qualifying the mode of cracking.

For the purpose of comparing fatigue initiation properties between axial and shear strain controlled conditions, like modes of failure must be considered. Therefore, for this discussion, failure in the torsional tests is defined as that point where a crack exists that is opening and closing. This appeared to coincide with the occurrance of a through thickness (4 mm) crack, causing a drop in the load amplitude required to maintain strain levels. Although the actual percentage of load drop at the point considered failure varied slightly for each specimen, it was typically between 10 and 20%. Any error introduced by this variance is slight since the load drop off is rapid after its onset.

Figures 11(a) - (c) show the stress-strain response of a specimen tested at a strain amplitude of $\gamma_a = \pm .025$. The first cycle of amplitude $\gamma_a = \pm .025$ shows distinct upper and lower yield points of 267 and 208 MPa. From there on the hysteresis loops assume the smooth shape similar to that seen in axial stress-strain response. Fig. 11(c) shows the hysteresis loop that was nearest to the half-life of the specimen.

Table IV lists the results of all fatigue tests. In all cases the stress amplitude was measured at the half-life where it was assumed that the stress-strain response was stable. Where possible, the shear modulus, G, was calculated with the data acquired in the first ramp to yield. The average shear modulus for the 17 tests was 79100 MPa. Elastic strain was calculated by dividing the shear modulus into the shear stress amplitude, and then subtracted from the total shear strain to get the plastic shear strain, or

$$\frac{\Delta\gamma_p}{2} = \frac{\Delta\gamma}{2} - \frac{\tau_a}{G} \tag{14}$$

The fatigue properties were obtained by linear regression of Eqs. 9(a) - 9(c). Figures 12(a) - (c) shows the results graphically.

From this group of data the specimens with the median life at each shear strain amplitude, along with the one long life test, were regressed separately as shown in Table V and Fig. 13(a).

The cyclic stress-strain curve in torsion is superimposed on the monotonic curve in Fig. 14. Mixed mode cyclic softening and hardening behavior is observed as it is in axial conditions.

Table VI shows a comparison of the fatigue properties in the axial and torsional cases. Included in this table are the transition fatigue lives, where the elastic and the plastic strains are equal.

A crude representation of the monotonic curve is shown in Fig. 15. The specimen buckled before final failure could be achieved. Table VII lists the relatively few data points available from the monotonic test in the high strain region.

B. Surface Phenomena Observed

The reporting of torsional fatigue tests results would not be complete without describing the surface cracking phenomena that occur long before any load drop off can be detected. Small (.25 mm) longitudinal cracks were detected on the surface throughout the gage length early in each test. As the early cracks grew to approximately 1 mm in length, many other smaller cracks continued to appear. However, it appeared that the majority of the cracks remained small while relatively few continued to grow to the 2 and 3 mm lengths. Near the end of a test, many of the cracks joined, greatly increasing the apparent crack propagation rate. Finally, a crack would propagate through the wall thickness. Figure 16 shows the magnetic particle enhanced gage length of specimen number 20 tested at $\gamma_a = \pm .025$. It shows one through-thickness crack which caused the load drop off and many of the lesser cracks not associated with final failure.

Figures 17(a) - (f) show the progression of surface cracking at one specific location for a specimen tested at $\gamma_a = \pm .008$. These pictures were taken from the replicas made during the test. The horizontal streaks are grinding marks, while the primarily vertical lines are the longitudinal fissures. Note that the alignment of the cracks is along a plane of maximum shear stress, which also coincides with the rolling direction of the material. Any tensile stress normal to this plane is negligible. Note also the similarity in alignment of the surface cracks seen in Figs. 17(c) - (f) to that of the inclusions present in the microstructure seen in Fig. 8. A different area of a replica from the same specimen, where several cracks appear likely to join, is shown in Fig. 18.

One would expect that the presence of cracks would cause a load drop off. Actually the shear stress amplitude increased as the surface cracking became more extensive. In the particular example shown in Figure 17, the material cyclically softened between N = 1 and N = 259, with the shear stress range decreasing from approximately 415 to 383 MPa. Coincident with the detection of cracks at N = 259, the shear stress range began to increase until it reached 401 MPa at N = 5195. Failure of this specimen was recorded at N = 5505 (2N = 11,010) due to a detected load drop off. Note that the life to detection of a significant surface crack in shear was only 5% of the total failure life. This pattern of surface cracking was exhibited by all the specimens, although the degree of surface cracking and when it was detected relative to

total life was dependent on the shear strain amplitude. The surface cracks were often long compared to the wall thickness. A surface crack on specimen number 14 (tested at $\gamma_a = \pm .005$) was directly observed through a microscope growing from 5 mm to 23 mm in total length before any load drop off occurred.

IV. DISCUSSION

The shear strain controlled data presented here shows a good fit to the power law fatigue relationships as written in terms of a torsional stress state. This result alone enhances the prospect of extrapolating the axial strain-based fatigue methodology into multiaxial situations. Even more promising is the comparison of the three fatigue exponents between torsional and axial stress states.

Within the context of normal scatter of fatigue data, the exponents in the torsional and axial states are essentially equal. It is important to realize that including or excluding any one data point will somewhat change the numerical values of b, c, and n'. However, the change should be slight if enough good data covering an adequate life range for analysis are used. With the two data sets reduced here, the exponents in torsion are within 6% of the axial values.

Assuming constant exponents, one might try to predict torsional fatigue response using fatigue shear ductility and shear strength coefficients derived from the axial properties and an equivalent stress criterion. Using the Tresca ($\tau_f' = \sigma_f'/2$ and $\gamma_f' = 1.5\ \varepsilon_f'$) or the von Mises ($\tau_f' = \sigma_f'/\sqrt{3}$ and $\gamma_f' = \sqrt{3}\ \tau_f'$) criterion, the predicted shear strength and ductility coefficients would envelope the values determined from the actual torsional fatigue data. The cyclic shear stress - shear strain curve and the total shear strain - life curve obtained from these criteria are shown graphically in Figs. 13(b) and (c), along with the torsional fatigue raw data points.

The presence of surface cracks with no corresponding load drop suggests that more attention must be given to establishing and defining failure criteria for multiaxial fatigue than for uniaxial. For the higher shear strain amplitudes tested here, surface cracks existed for nearly the entire life of the specimen. Yet, a crack propagation approach seems impractical to apply at the early stages due to the vast number of cracks apparently growing at different rates.

The longitudinal growth of these cracks, i.e., on planes of negligible tensile stress, verifies the occurrence of the shear mode of failure. As mentioned earlier, the stress amplitude typically increased slightly as this early surface cracking became more extensive. It is unclear whether the stress increase caused the surface cracking or vice versa.

These experimental results suggest many future research topics. Undoubtably, any future investigator in the area of multiaxial fatigue will be faced with the problems of defining failure, defining initiation versus propagation in different modes and handling the existence of a large number of cracks, some propagating and others non-propagating.

V. CONCLUSIONS

The experimental results presented here support the following conclusions:

1. Shear strain controlled fatigue data may be reduced with the same power law relationships as in the axial case.
2. The steel tested exhibits cyclically mixed mode behavior in torsional fatigue, i.e., it cyclically softens at low strain amplitudes and cyclically hardens at high strain amplitudes.
3. The fatigue strength exponent, b, cyclic strain hardening exponent, n', and the fatigue ductility exponent, c, are independent of the stress states tested for like modes of failure for 1045 HR and normalized steel.
4. The inclusions in this steel probably act as initiation sites for the longitudinal shear cracks.
5. Relatively large surface cracks in shear exist during a significant portion of the full load carrying lifetime.

TABLES

TABLE I

CHEMICAL COMPOSITION OF 1045 STEEL

Chemical Analysis From Optical Emission Spectroscopy.

(Courtesy Deere & Company Technical Center, Moline, IL)

C	Mn	P	S	Si	Ni	Cr	Mo	Cu	Al
.44	.70	.019	.046	.23	.03	.05	Nil	.03	.05

B	V	Nb	Pb	Ti
.0002	.002	.008	.005	.002

TABLE II

AXIAL MONOTONIC PROPERTIES OF 1045 STEEL

(Courtesy Deere & Company Technical Center, Moline, IL)

ID	BHN	σ_y (MPa)	σ_f (MPa)	ε_f	%RA	E (MPa)	n	K (MPa)
M022	157	384	992	.71	51	203350	.23	1197
M104	148	379	977	.71	51	201400	.23	1172
Average	153	382	985	.71	51	202375	.23	1185

TABLE III

AXIAL FATIGUE INITIATION DATA AND PROPERTIES

(Raw Data Provided by Deere & Company Technical Center, Moline, IL)

E = 202375 MPa	σ_f' = 948 MPa
K' = 1258 MPa	b = -.092
n' = .208	ε_f' = .260
	c = -.445

Total Strain Amplitude	Stress Amplitude (MPa)	Plastic Strain Amplitude	Reversals to Failure
.0200	524	.01741	514
.0150	499	.01253	770
.0100	452	.00777	3054
.0100	465	.00770	2922
.0080	445	.00581	6088
.0080	440	.00583	4093
.0060	400	.00402	13344
.0060	420	.00393	13650
.0050	372	.00316	25826
.0040	351	.00227	35970
.0040	353	.00226	40398
.0030	315	.00144	73860
.0025	298	.00103	234268
.0020	270	.00067	523222
.0020	269	.00067	762902
.0015	241	.00031	4901750

TABLE IV

TORSIONAL FATIGUE INITIATION DATA AND PROPERTIES

$\tau_f' = 505$ MPa		$b_o = -.097$	
$\gamma_f' = .413$		$c_o = -.445$	
$K_o' = 615$ MPa		$n_o' = .219$	
Shear Strain	Shear Stress (MPa)	Shear Modulus (MPa)	Plastic Shear Strain	Reversals to Load Drop Off	Specimen No.
.0250	272	80200	.0216	940	20
.0251	270	78200	.0216	990	18
.0250	259	80100	.0218	1082	16
.0150	232	78400	.0120	2538	1
.0150	237	78200	.0120	2758	6
.0150	232	78100	.0120	2934	13
.0150	235	78400	.0120	--	2*
.0082	198	81200	.0058	11010	12
.0082	200	80400	.0057	14264	3
.0082	194	79100	.0057	16716	4
.0060	186	78400	.0036	22146	5
.0050	161	78000	.0029	60746	11
.0050	165	78000	.0029	70036	14
.0050	168	78300	.0029	72234	15
.0041	160	81200	.0021	83678	7**
.0040	159	78000	.0020	145928	10
.0039	154	78200	.0019	190536	9
.0030	148	80700	.0012	1092006	8

*Test aborted due to hydraulics failure.

**Test interrupted due to lack of agreement between RVDT and rosette. Specimen and RVDT reset.

TABLE V

TORSIONAL FATIGUE INITIATION DATA AND PROPERTIES
USING MEDIAN LIFE RESULTS

	$\sigma_f' = 481$ MPa	$b_o = -.090$	
	$\gamma_f' = .340$	$c_o = -.419$	
	$K_o' = 614$ MPa	$n_o' = .217$	
Total Shear Strain	Shear Stress (MPa)	Shear Modulus (MPa)	Plastic Shear Strain	Reversals to Load Drop Off	Specimen No.
.0251	270	78200	.0216	990	18
.0150	237	78200	.0120	2758	6
.0082	200	80400	.0057	14264	3
.0050	165	78000	.0029	70036	14
.0040	159	78000	.0020	145928	10
.0030	148	80700	.0012	1092006	8

TABLE VI

SUMMARY OF FATIGUE INITIATION PROPERTIES

Fatigue Property	Stress State		
	Axial	Torsional (17 Test Points)	Torsional (6 Test Points)
b	-.092	-.097	-.090
n'	.208	.219	.217
c (as regressed)	-.445	-.445	-.419
$c = b/n'$	-.442	-.443	-.415
K' (MPa) (as regressed)	1258	615	614
σ_f' or τ_f' (MPa)	948	505	481
ε_f' or γ_f'	.260	.413	.340
$2N_t$	87,382	159,790	204,919

TABLE VII

TORSIONAL MONOTONIC RESULTS OF 1045 STEEL

(Estimates of Post Yield Results)

Shear Strain Amplitude	Shear Stress Amplitude (MPa)	Remarks
.083	344	
.227	406	
.349	421	
.415	438	Visible buckling occurred
.576	473	Gross specimen buckling occurred

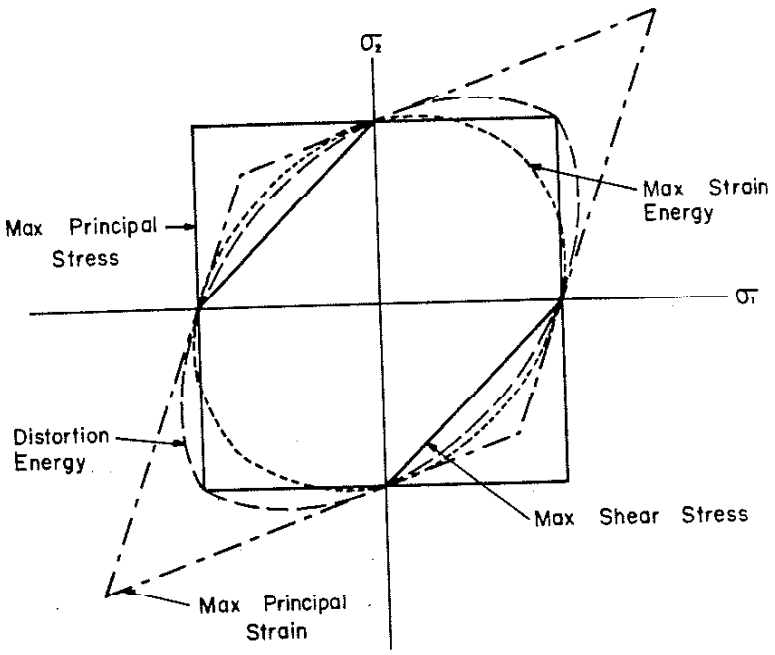

Fig. 1 Static/Equivalent Stress Criteria

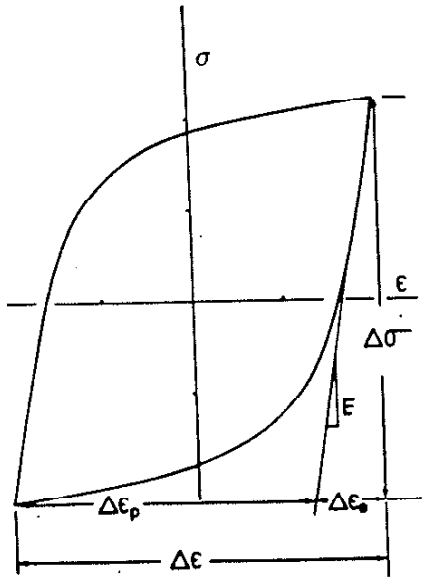

Fig. 2 Stable Axial Hysteresis Loop

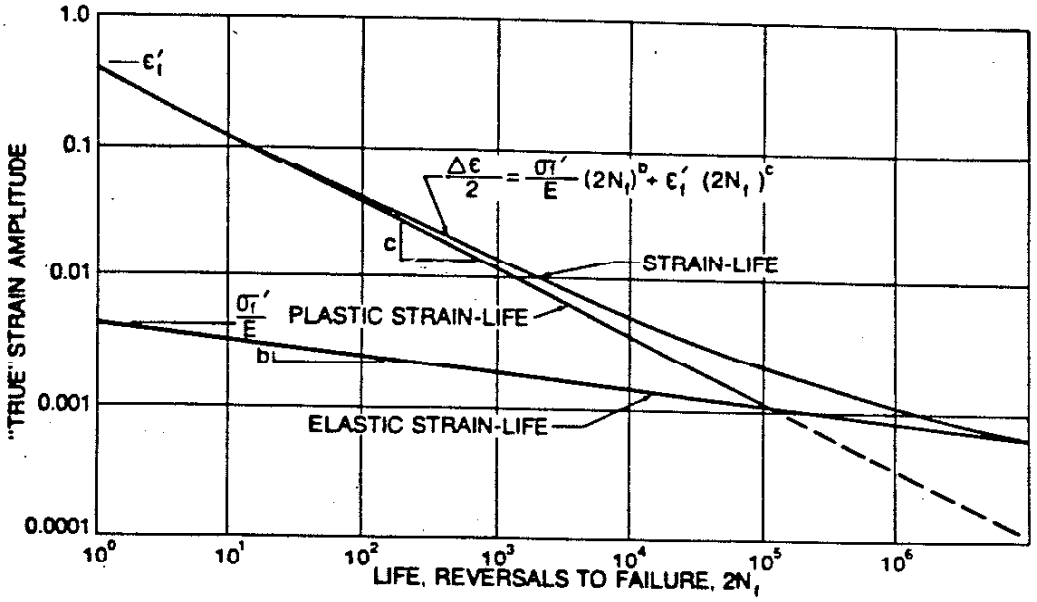

Fig. 3 Strain-Life Curve for a Mild Steel

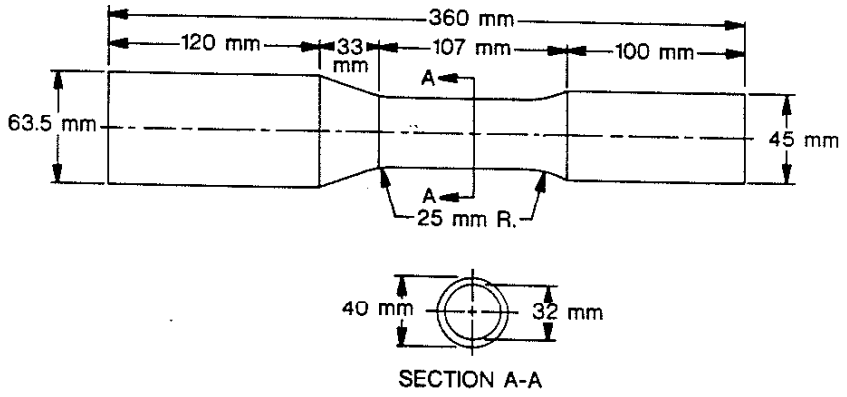

Fig. 4 Torsional Fatigue Specimen

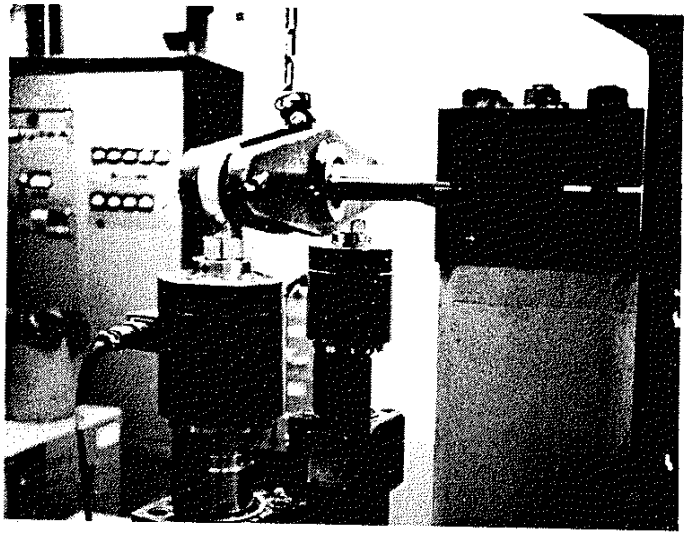

Fig. 5(a) Test Apparatus, Side View

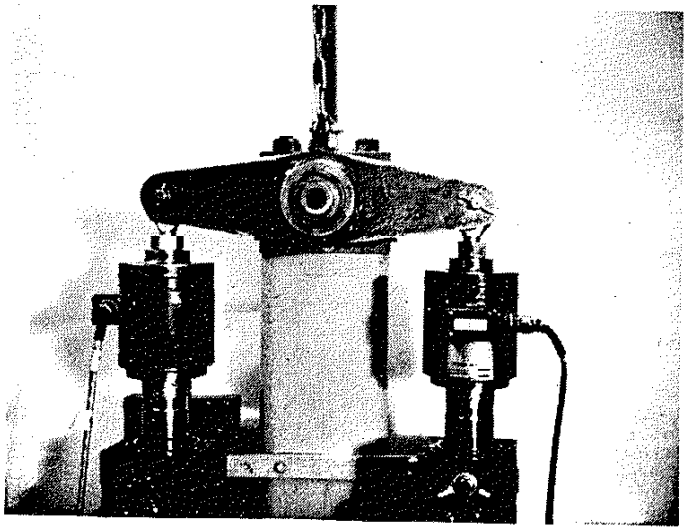

Fig. 5(b) Test Apparatus, End View

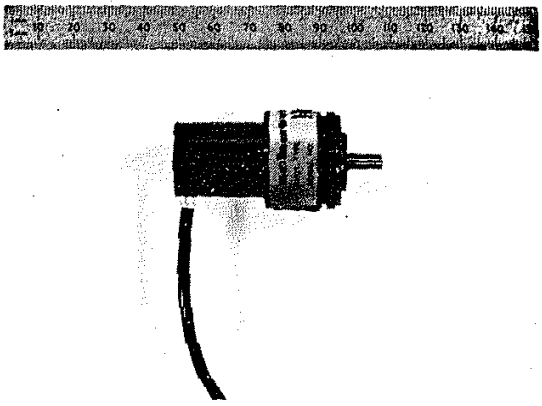

Fig. 6(a) Rotary Variable Differential Transducer (RVDT)

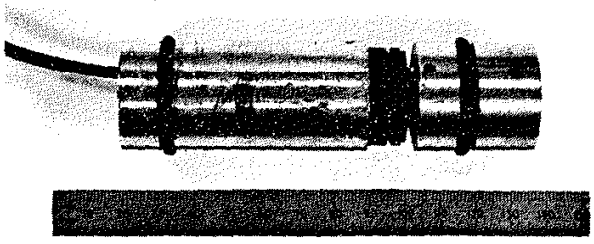

Fig. 6(b) Shear Strain "Extensometer"

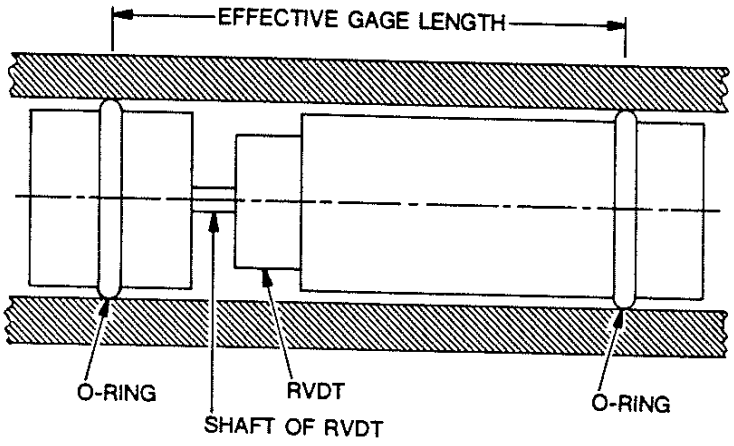

Fig. 7 Shear Strain Extensometer Positioned in Specimen Gage Length

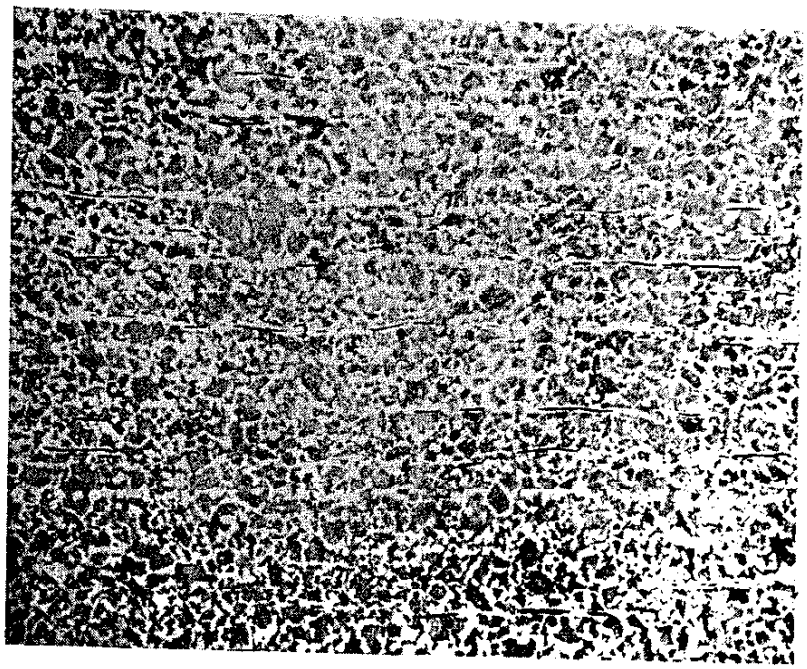

Fig. 8 Microstructure of Steel Used (Magnification = 100X. Picture courtesy of D. Brodd, Deere & Company Technical Center, Moline, IL)

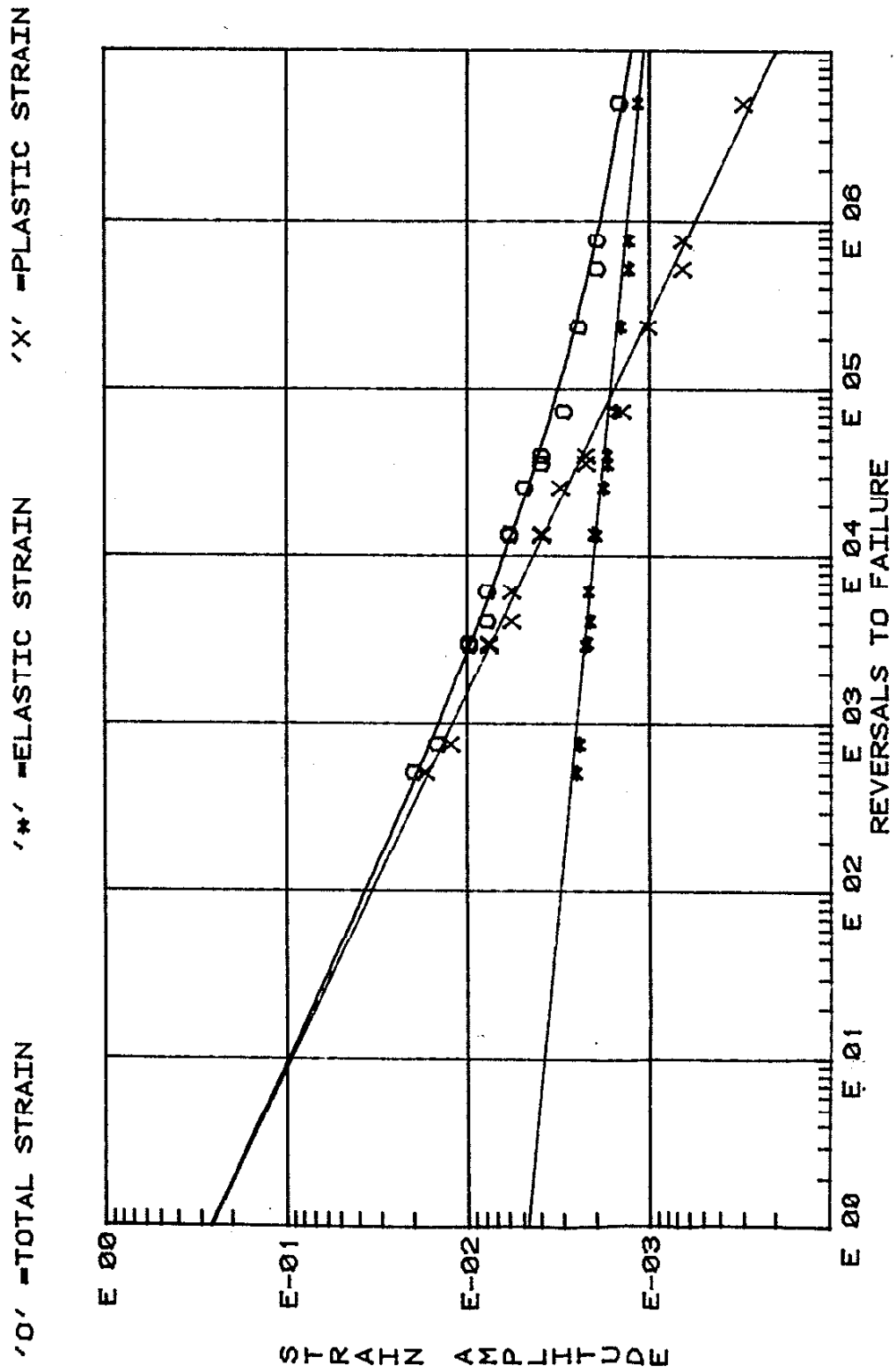

Fig. 9 Axial Total Strain versus Life of Steel Used

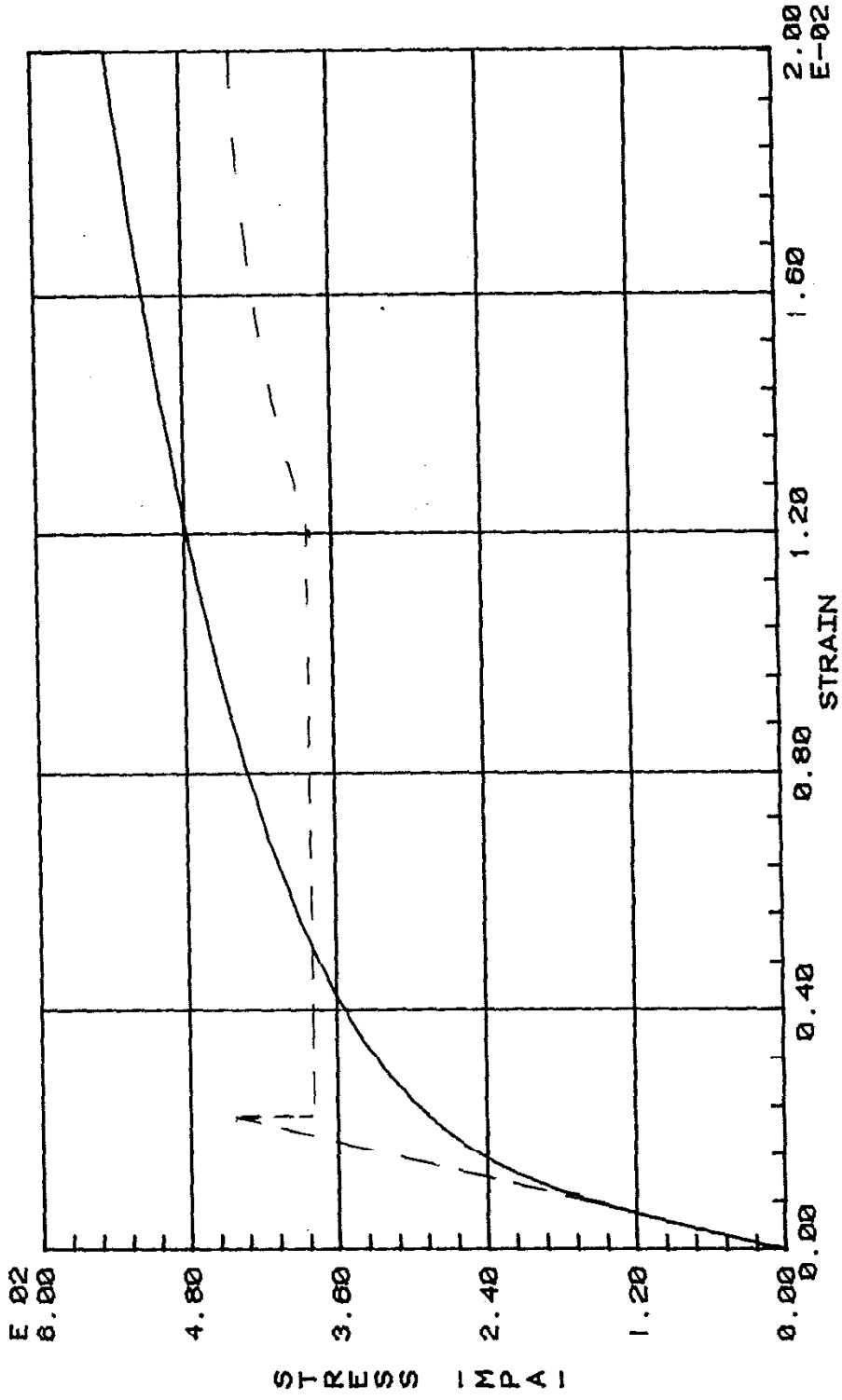

Fig. 10 Axial Monotonic and Cyclic Stress versus Strain Curves

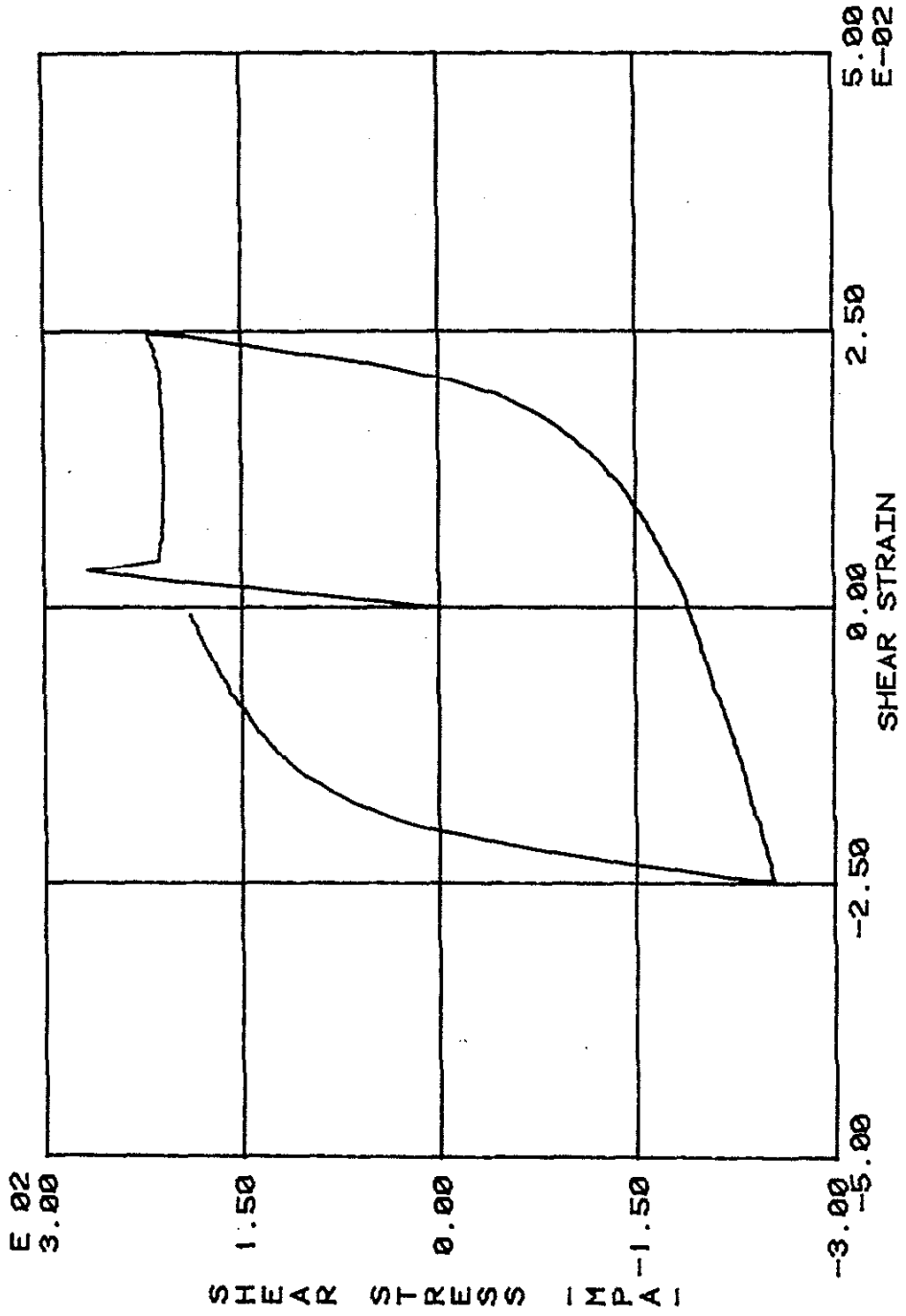

Fig. 11(a) Shear Stress versus Shear Strain, Specimen #20, N = 1, $\gamma_a = \pm .025$

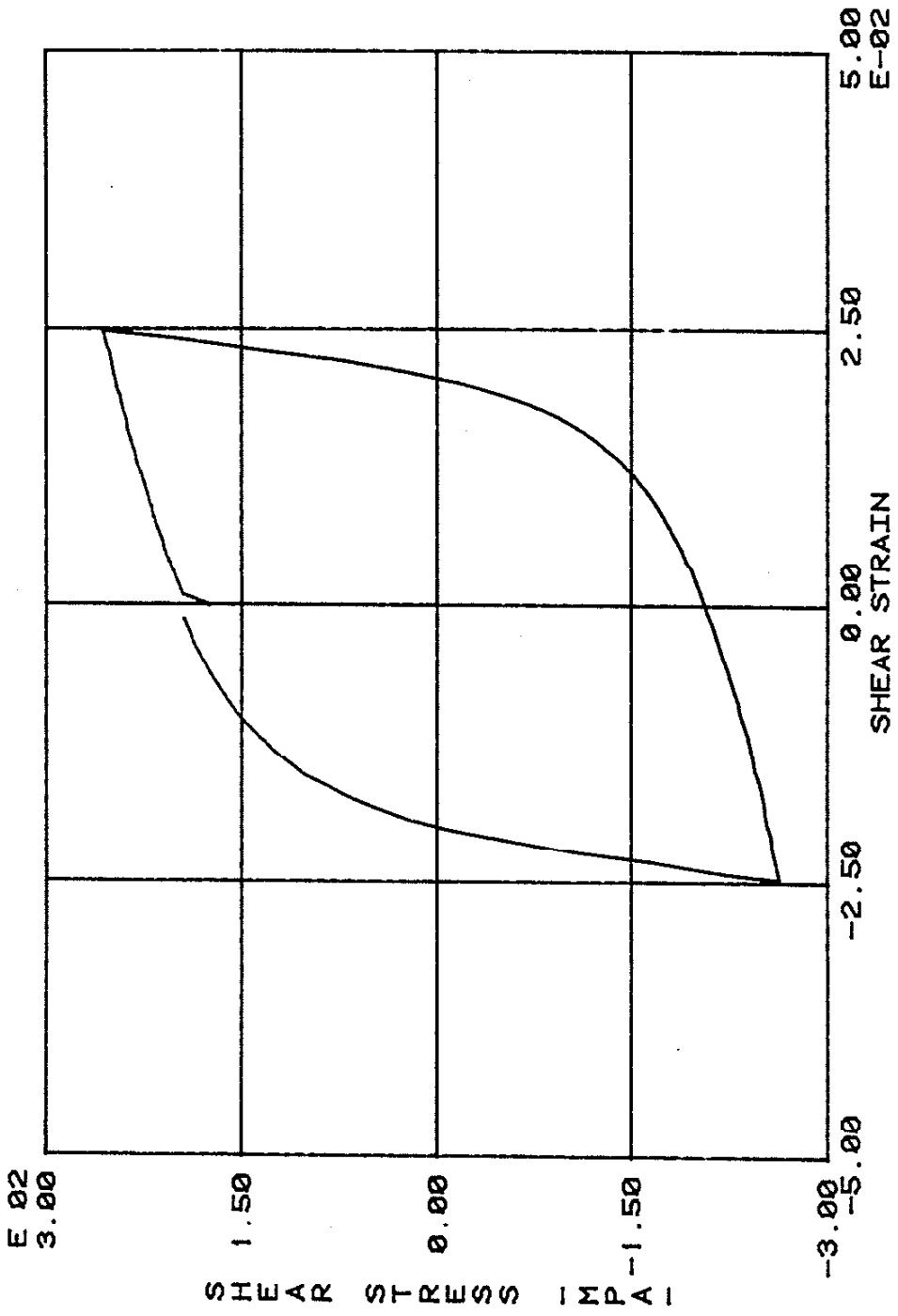

Fig. 11(b) Shear Stress versus Shear Strain, Specimen #20, N = 2, $\gamma_a = \pm .025$

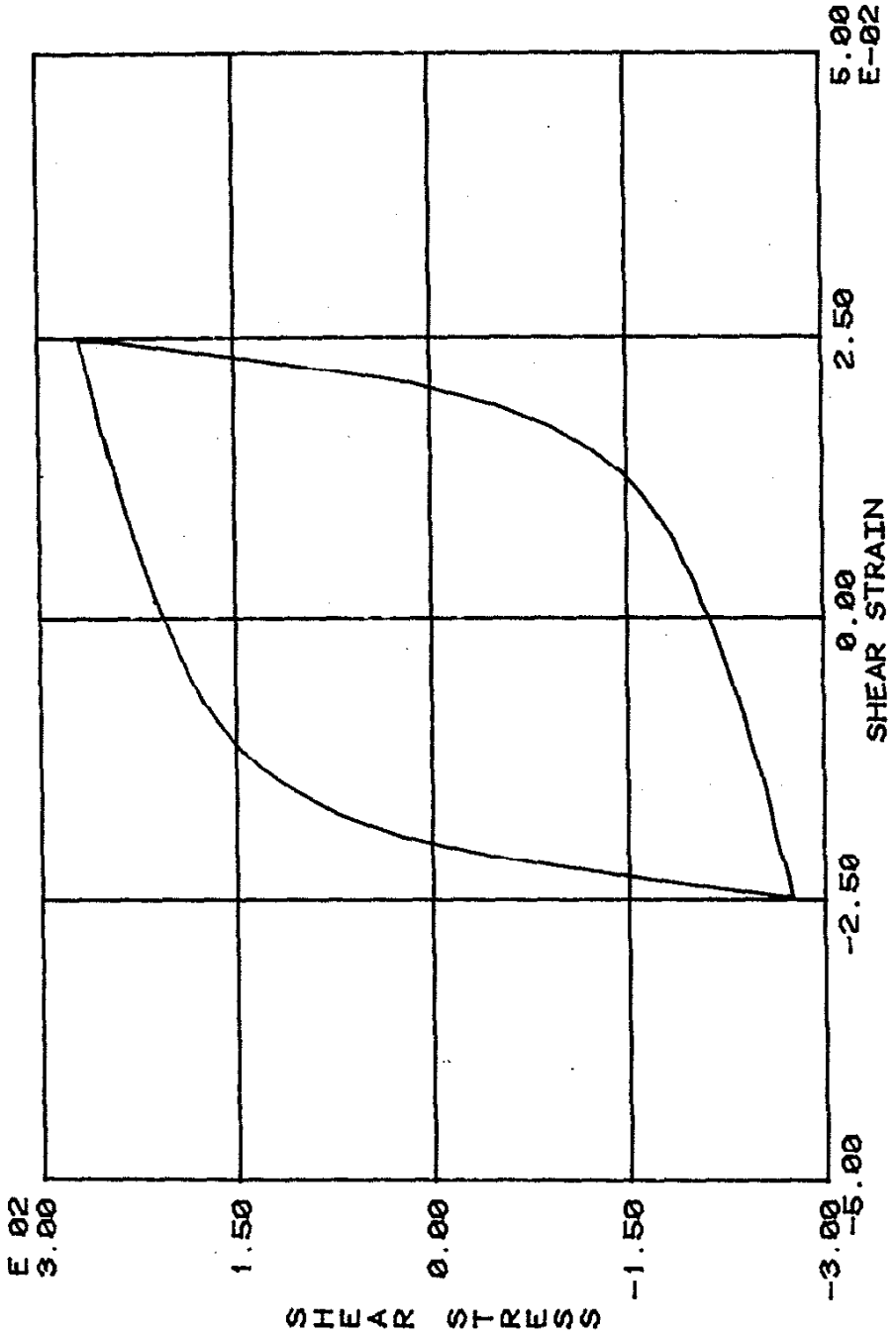

Fig. 11(c) Stabilized Hysteresis Loop, Specimen #20, N = 259, $\gamma_a = \pm .025$

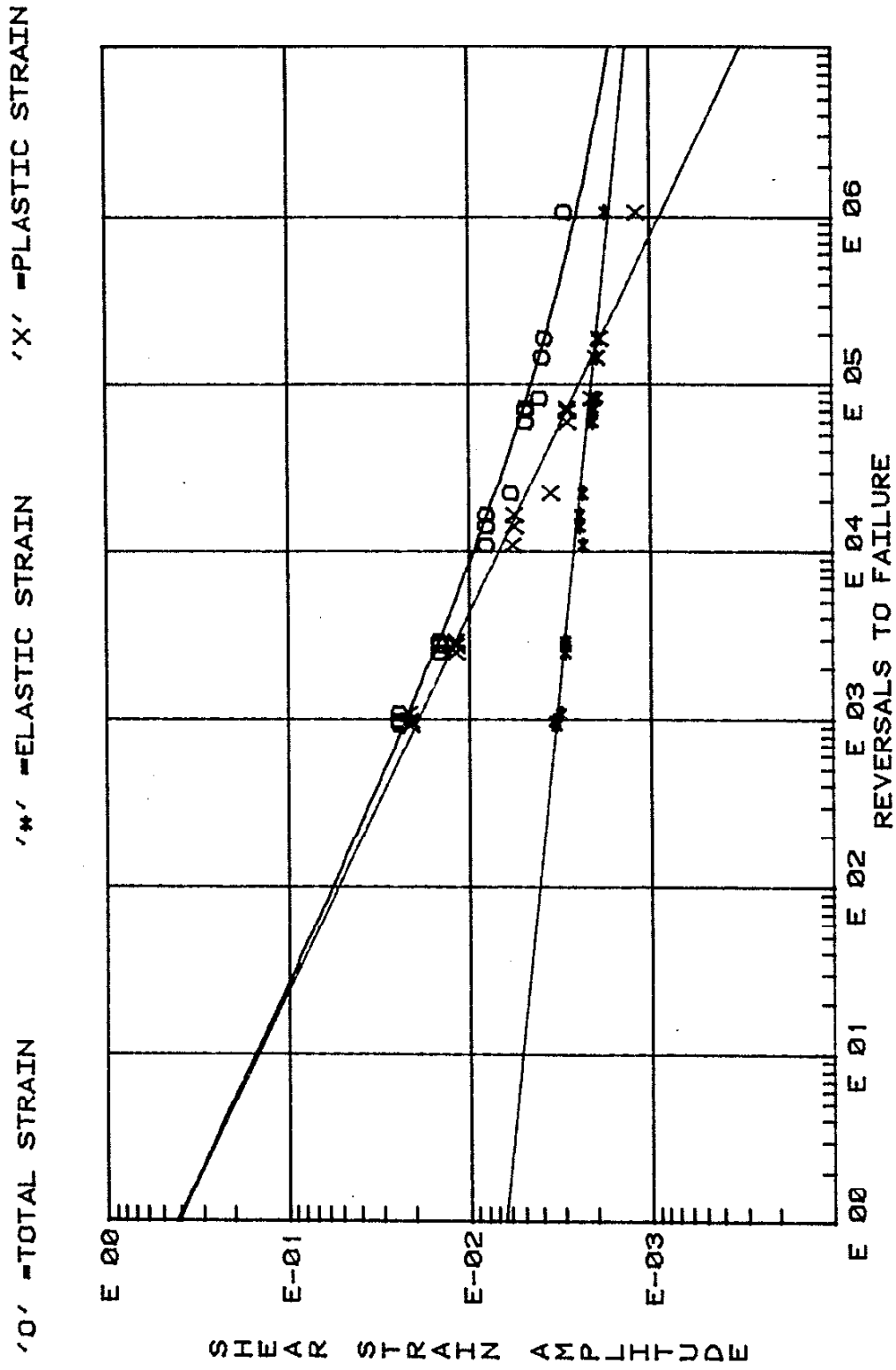

Fig. 12(a) Total Shear Strain versus Reversals to Failure

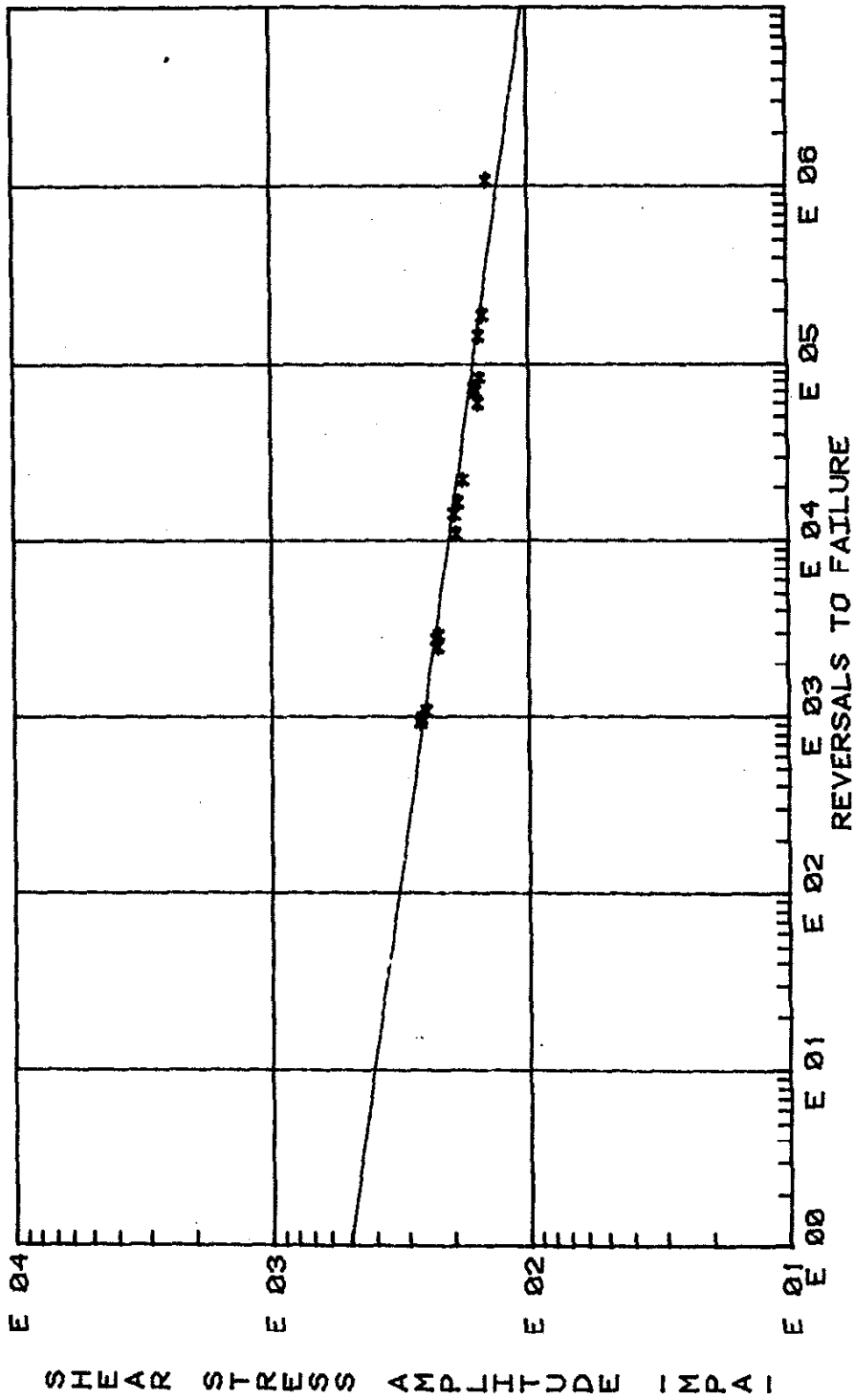

Fig. 12(b) Shear Stress versus Reversals to Failure

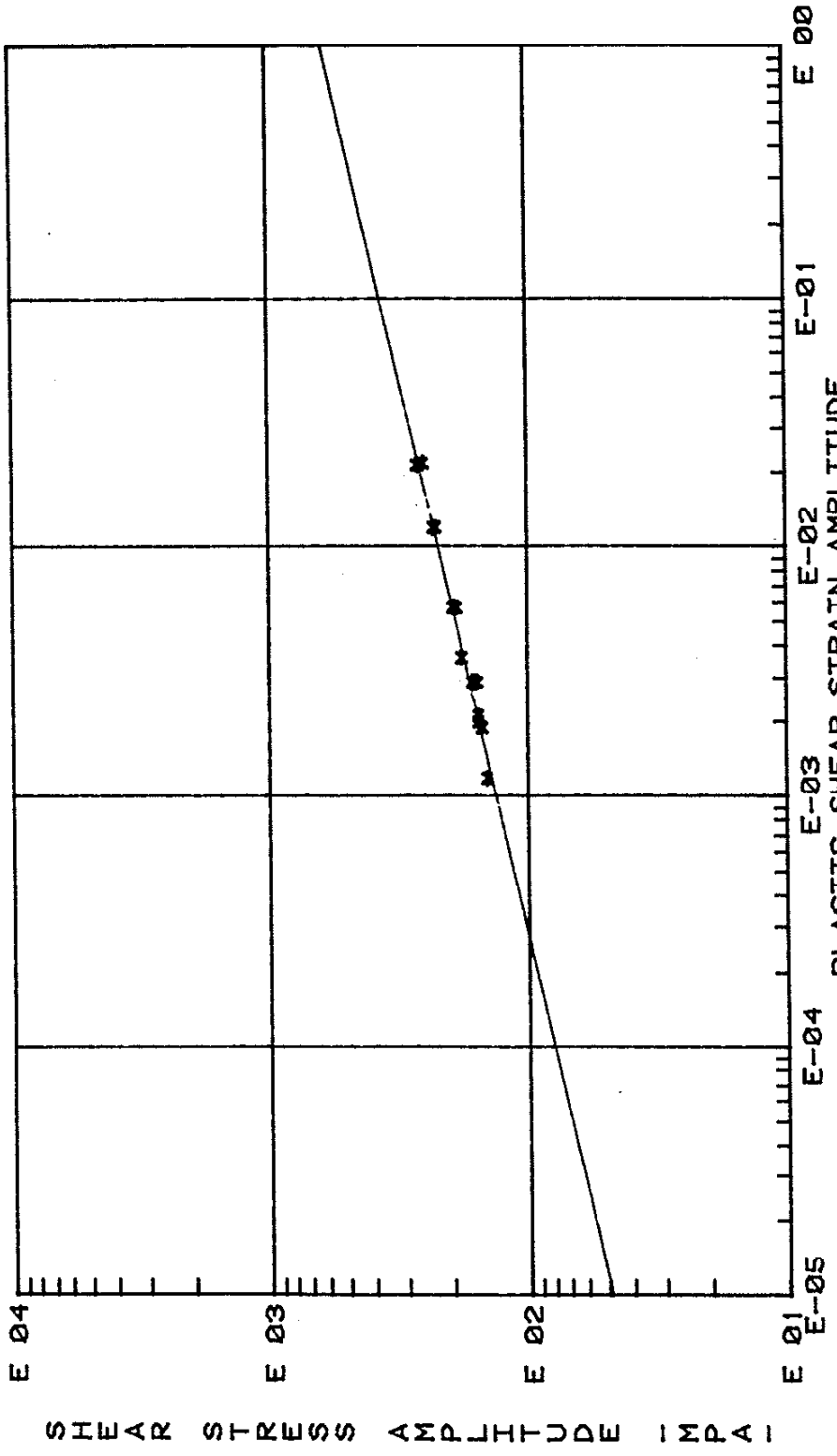

Fig. 12(c) Shear Stress versus Plastic Shear Strain

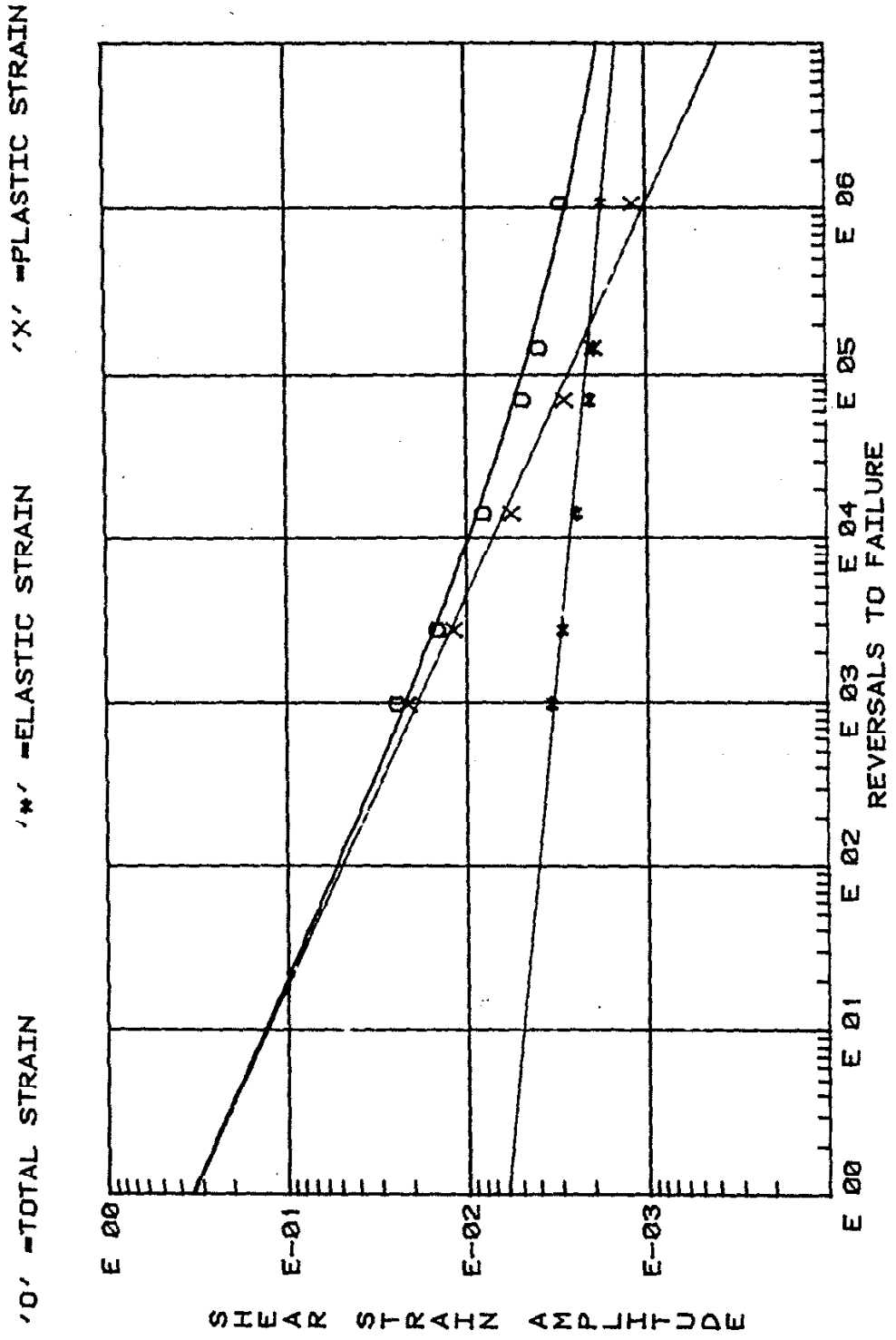

Fig. 13(a) Total Shear Strain versus Reversals to Failure (Median Life Data)

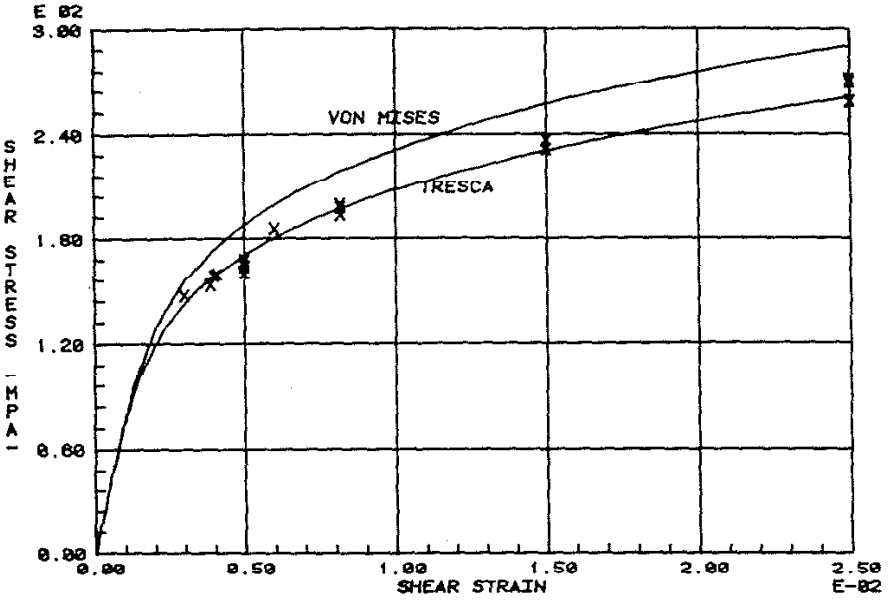

Fig. 13(b) Shear Stress versus Shear Strain
as Predicted with Tresca and vonMises Criteria

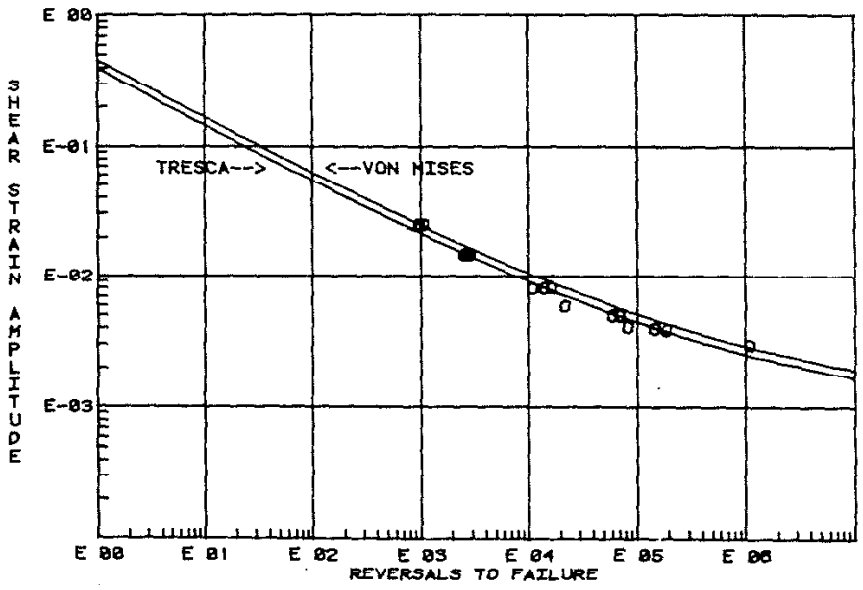

Fig. 13(c) Total Shear Strain versus Reversals to Failure
as Predicted with Tresca and vonMises Criteria

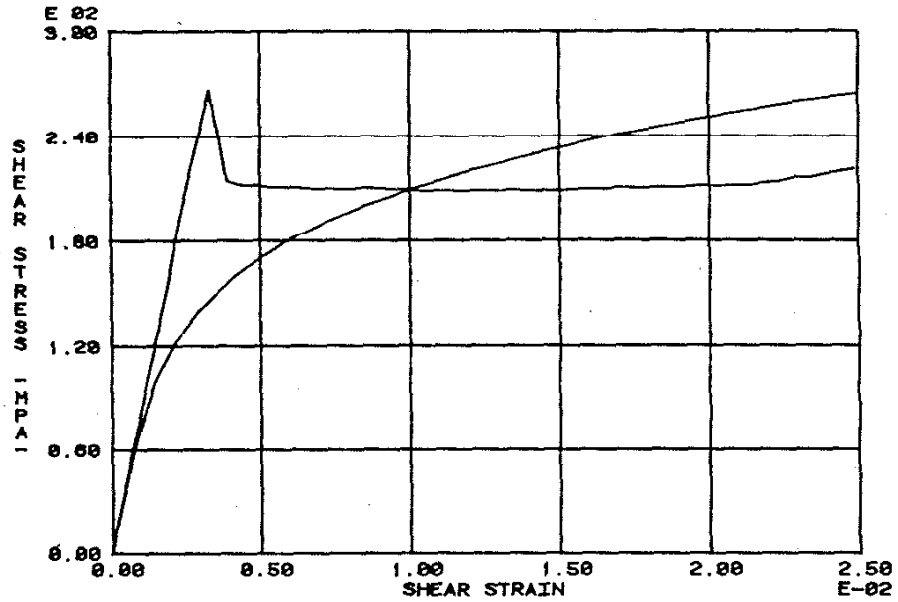

Fig 14. Monotonic and Cyclic Shear Stress versus Shear Strain

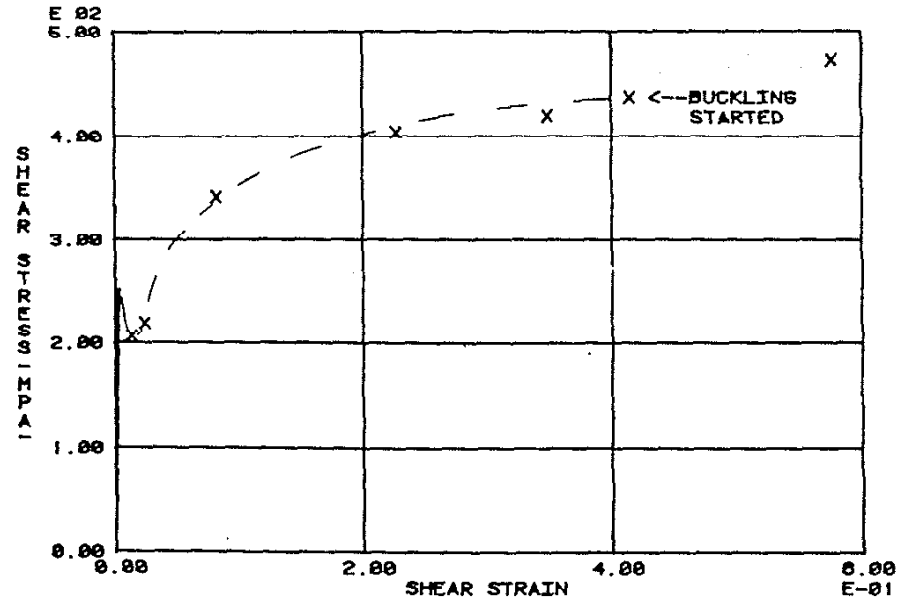

Fig 15. Estimated Monotonic Shear Stress versus Shear Strain

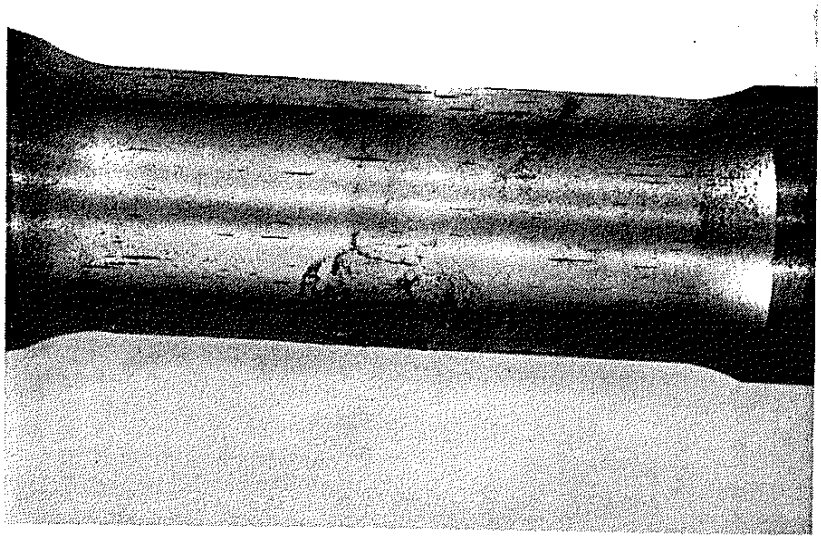

Fig. 16 Magnetic Particle Enhanced Gage Length of Specimen #20 (Picture courtesy of D. Brodd, Deere & Company Technical Center, Moline, IL)

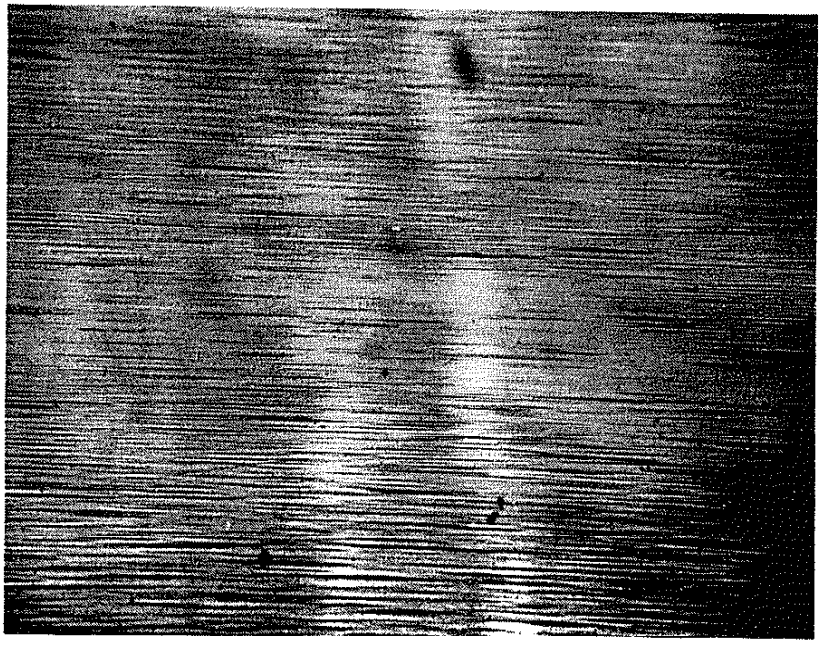

Fig. 17(a) Replica of Specimen #12, N = 0 ($\gamma_a = \pm .008$, Magnification = 50X)

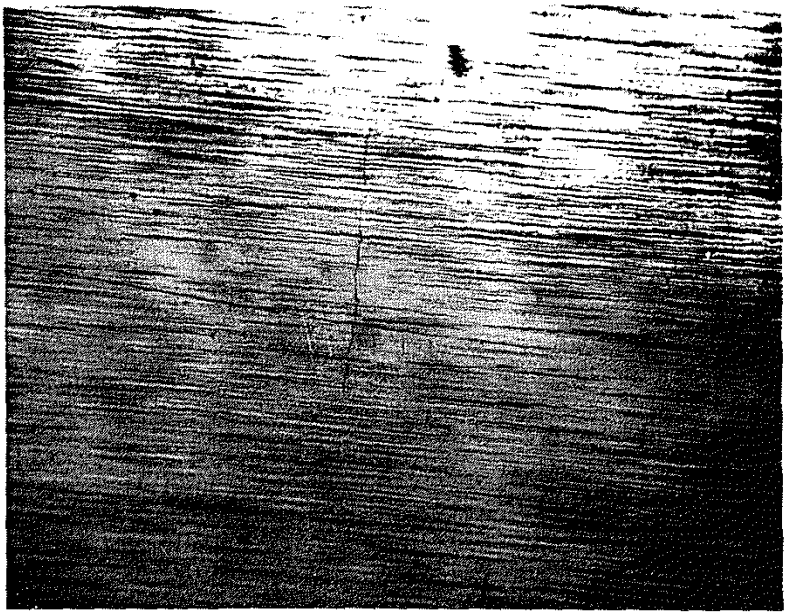

Fig. 17(b) Replica of Specimen #12, N = 259
(γ_a = ± .008, Magnification = 50X)

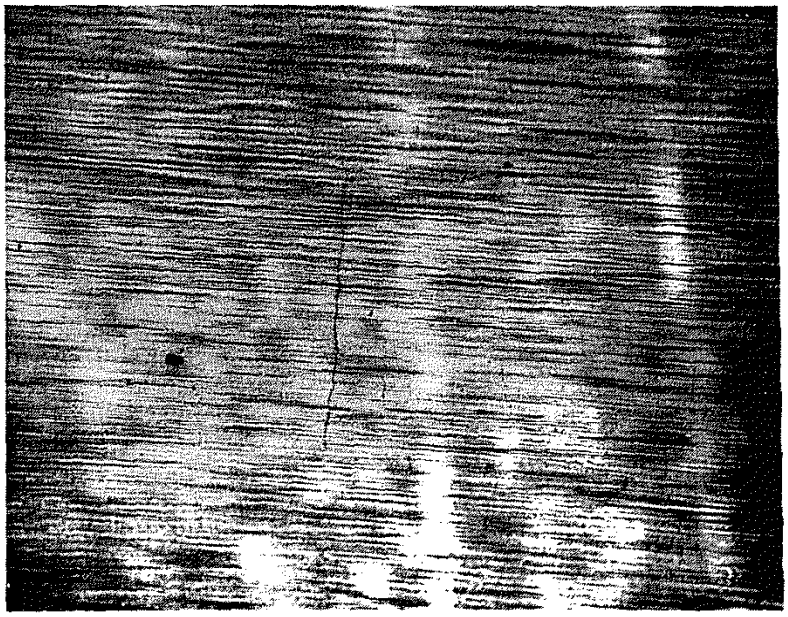

Fig. 17(c) Replica of Specimen #12, N = 540
(γ_a = ± .008, Magnification = 50X)

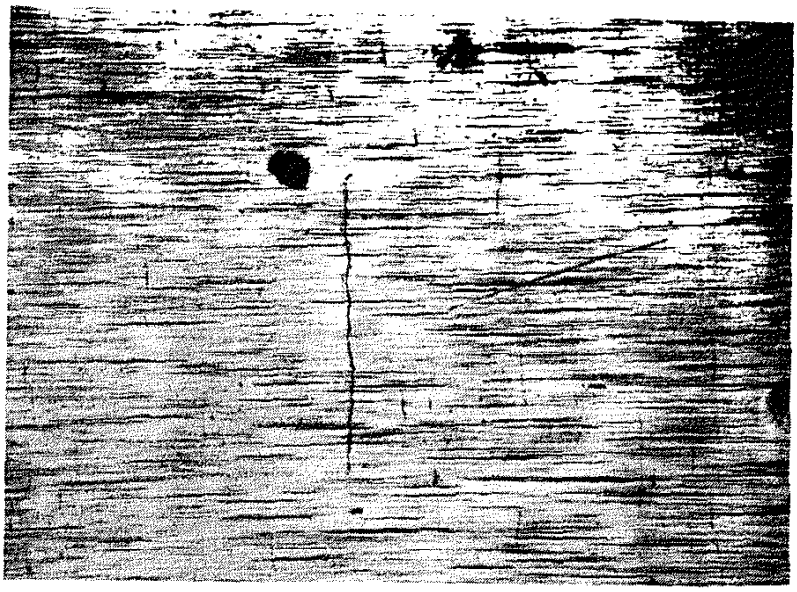

Fig. 17(d) Replica of Specimen #12, N = 1399
(γ_a = ± .008, Magnification = 50X)

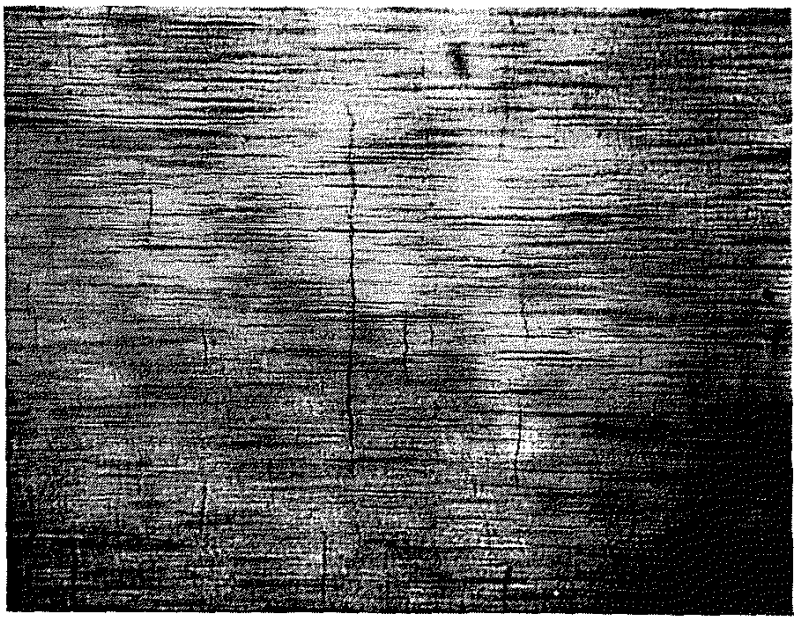

Fig. 17(e) Replica of Specimen #12, N = 4633
(γ_a = .008, Magnification = 50X)

Fig. 17(f) Replica of Specimen #12, N = 5195 (γ_a = ± .008, Magnification = 50X)

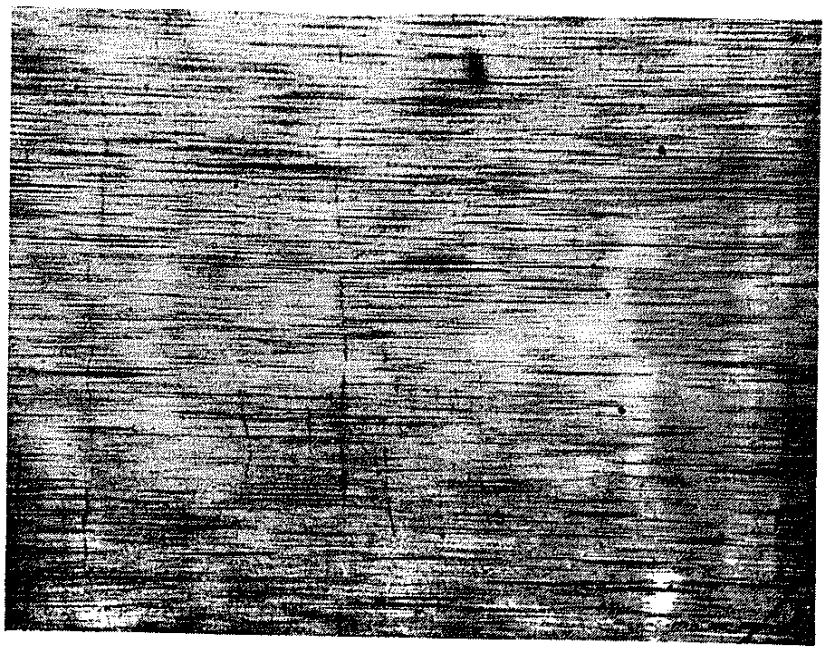

Fig. 18 Replica Showing Typical Surface Crack Alignment (Specimen #14, γ_a = ± .008, N = 4123, Magnification = 50X)

REFERENCES

1. Gough, H.J. and Pollard, H.V., "The Strength of Metal under Combined Alternating Stresses", Proceedings of the Institution of Mechanical Engineers, London, Vol. 131, 1935, pp. 3-103.

2. Garud, Y.S., "Multi-Axial Fatigue: A Survey of the State of the Art", Department of Mechanical Engineering, Stanford University. For presentation at the ASTM/SAE Workshop on "Elasto-Plastic Materials Behavior and Component Fatigue Analysis", April 1980.

3. Findley, W.N., Coleman, J.J. and Hanley, B.C., "Theory for Combined Bending and Torsion Fatigue with Data for SAE 4340 Steel", International Conference on Fatigue of Metals, November 1956.

4. McDiarmid, D.L., "A General Criterion of Fatigue Failure under Multi-Axial Stress", Department of Mechanical Engineering, The City University, London, England.

5. Sines, G. and Waisman, J.L., Metal Fatigue, McGraw-Hill Book Co., 1959, pp. 145-167.

6. Sines, G., "Failure of Materials under Combined Repeated Stresses with Superimposed Static Stresses", National Advisory Committee for Aerodynamics, Technical Note 3495 (1955).

7. Morrow, JoDean, "Cyclic Plastic Strain Energy and Fatigue of Metals", Internal Friction, Damping and Cyclic Plasticity, ASTM STP No. 378, 1965, pp. 45-87.

8. Morrow, JoDean, Wetzel, R.M., and Topper, T.H., "Laboratory Simulation of Structural Fatigue Behavior," Effects of Environment and Complex Load History on Fatigue Life, ASTM STP 462, American Society for Testing and Materials, 1970, pp. 74-91.

9. Socie, D.F., Mitchell, M.R. and Caulfield, E.M., Fundamentals of Modern Fatigue Analysis, FCP Report No. 26, College of Engineering, University of Illinois, Urbana, IL, January 1978.

10. Pascoe, K.J. and deVilliers, J.W.R., "Low Cycle Fatigue of Steels under Biaxial Straining", Journal of Strain Analysis, Vol. 2, No. 2, 1967, pp. 117-126.

11. Taira, S., Inoue, J. and Takahashi, M., "Low Cycle Fatigue under Multiaxial Stresses (In the Case of Combine Cyclic Tension-Compression and Cyclic Torsion in the Same Phase at Elevated Temperature)", The 10th Japan Congress on Testing Materials--Metallic Materials, March 1967, pp. 18-23.

12. Taira, S., Inoue, J., and Yoshida, T., "Low Cycle Fatigue under Multiaxial Stresses (In the case of Combined Cyclic Tension-Compression and Cyclic Torsion at Room Temperature") The 12th Japan Congress on Materials Research -- Metallic Materials, March 1969, pp. 50-55.

13. Taira, S., Inoue, J., and Yoshida, T., "Low Cycle Fatigue under Multiaxial Stresses (In the Case of Combined Cyclic Tension-Compression and Cyclic Torsion Out-of-Phase at Elevated Temperature)", The 11th Japan Congress on Materials Research -- Metallic Materials, March 1968, pp. 60-65.

14. Havard, D.G. and Topper, T.H., "Low-Cycle Biaxial Fatigue of AISI 1018 Steel", Ontario Hydro Research Quarterly, 2nd Quarter, 1969, pp. 1-12.

15. Havard, D.G., Williams, D.P. and Topper, T.H., "Biaxial Fatigue of Mild Steel: Data Synthesis and Interpretation", Ontario Hydro Research Quarterly, Second Quarter, 1975, pp. 11-18.

16. Mowbray, D.F., "A Hydrostatic Stress-Sensitive Relationship for Fatigue under Biaxial Stress Conditions", Journal of Testing and Evaluation, Vol. 8, No. 1, pp. 3-8.

17. Halford, G.R. and Morrow, JoDean, "Low Cycle Fatigue in Torsion", T.&A.M. Report No. 203, Department of Theoretical and Applied Mechanics, University of Illinois, October 1961.

18. "Technical Report on Fatigue Properties - SAE J1099", SAE Handbook 1980, Part 1, Society of Automotive Engineers, Inc., 1980, pp. 4.50-4.51,.

19. Benham, P.P., "Axial-Load and Strain-Cycling Fatigue of Copper at Low Endurance", Journal of Mechanical Engineering Science, Vol. 89, 1961, pp. 328-338.

20. Benham, P.P., "Torsional Strain-Cycling Fatigue of Copper at Low Endurance", Journal of the Institute of Metals, Vol. 91, 1962-63, pp. 404-407.

21. Nadai, A., Theory of Flow and Fracture of Solids, 2nd Edition, Vol. I, McGraw-Hill Book Company, New York, 1950, pp. 347-349.

22. Galliart, D.R. and Downing, S.D., "A Fatigue Test Program for a Notched Round Component", submitted for publication to the ASTM Symposium on Biaxial/Multiaxial Fatigue, San Francisco, December, 1982.

23. Curless, G.L. (Deere & Company Technical Center, Moline, IL), Personal Communication, 1982.

24. Penfold, G.F. (Deere & Company Technical Center, Moline, IL), Personal Communication, 1981.

PARTIAL LIST OF FRACTURE CONTROL PROGRAM REPORTS

REPORT NO.

23 "A UNIFIED PREDICTIVE TECHNIQUE FOR THE FATIGUE RESISTANCE OF CAST FERROUS-BASED METALS AND HIGH HARDNESS WROUGHT STEELS," MICHAEL ROGER MITCHELL, SEPTEMBER, 1976.

24 "REVIEW OF CONTEMPORARY APPROACHES TO FATIGUE DAMAGE ANALYSIS," D. F. SOCIE AND JODEAN MORROW, DECEMBER, 1976.

25 "MATERIAL CHARACTERIZATION OF SAE 950XK; MONOTONIC AND CYCLIC STRESS-STRAIN BEHAVIOR AND STRAIN-LIFE RESPONSE," MICHAEL ROGER MITCHELL, FEBRUARY, 1977.

26 "FUNDAMENTALS OF MODERN FATIGUE ANALYSIS," D. F. SOCIE, M. R. MITCHELL AND E. M. CAULFIELD, APRIL, 1977.

27 "MATERIAL CHARACTERIZATION OF A 1% NICKEL STEEL; MONOTONIC AND CYCLIC STRESS-STRAIN BEHAVIOR AND STRAIN-LIFE RESPONSE," MICHAEL R. MITCHELL AND RONALD B. ZWEIGORON, SEPTEMBER, 1977.

28 "EVALUATION OF FRACTURE MECHANICS PARAMETERS FOR A27 CAST STEEL," E. M. CAULFIELD, DECEMBER, 1977.

29 "THE EFFECT OF RESIDUAL STRESSES ON WELD FATIGUE LIFE," J. D. BURK AND F. V. LAWRENCE, JANUARY, 1978.

30 "CHARACTERIZATION OF DUCTILE FRACTURE IN WROUGHT STEELS AND WELDMENTS," E. P. COX, F. V. LAWRENCE AND G. M. SINCLAIR, JUNE, 1978.

31 "EFFECT OF SPECTRUM EDITING ON FATIGUE CRACK INITIATION AND PROPAGATION IN A NOTCHED MEMBER," DARRELL F. SOCIE AND PAUL J. ARTWOHL, DECEMBER, 1978.

32 "A MODEL FOR JOINING THE FATIGUE CRACK INITIATION AND PROPAGATION ANALYSES," W. C. CHEN AND F. V. LAWRENCE, NOVEMBER, 1979.

33 "FINITE ELEMENT SIMULATION OF THE MICROSTRUCTURE OF GRAY CAST IRON," EDWARD S. RUSSELL, DECEMBER, 1979.

34 "CYCLIC DEFORMATION AND FATIGUE BEHAVIOR OF CARBURIZED STEEL," JOHN M. WARANIAK, MAY, 1980.

35 "FATIGUE CRACK INITIATION AND GROWTH IN GRAY CAST IRON," JAMES W. FASH, OCTOBER, 1980.

36 "PREDICTING THE FATIGUE RESISTANCE OF WELDS," F. V. LAWRENCE, N. J. HO AND P. K. MAZUMDAR, OCTOBER, 1980.

37 "CYCLE COUNTING FOR VARIABLE AMPLITUDE CRACK GROWTH," DARRELL F. SOCIE AND PETER KURATH, APRIL, 1981.

38 "AN ANALYTICAL STUDY OF THE FATIGUE NOTCH SIZE EFFECT," P. K. MAZUMDAR AND F. V. LAWRENCE, APRIL, 1981.

39 "FATIGUE BEHAVIOR AND CRACK DEVELOPMENT IN COMPACTED GRAPHITE CAST IRON," LAWRENCE MOLINARO, MAY, 1981.

40 "FATIGUE OF LOW CARBON STEELS AS INFLUENCED BY REPEATED STRAIN AGING," HUSEYIN SEHITOGLU, JUNE, 1981.

41 "A DIMENSIONLESS INITIATION PARAMETER IN FATIGUE OF CARBURIZED STEEL," GOLAM M. NEWAZ, NOVEMBER, 1981.

42 "THE EFFECT OF SELECTED SUBCYCLES IN BLOCK LOADING FATIGUE HISTORIES," THOMAS J. DEVES, PETER KURATH, HUSEYIN SEHITOGLU AND JODEAN MORROW, MARCH, 1982.